

Golgi self-correction generates bioequivalent glycans to preserve cellular homeostasis

Haik Mkhikian¹, Christie-Lynn Mortales¹, Raymond W Zhou²,
Khachik Khachikyan¹, Gang Wu³, Stuart M Haslam³, Patil Kavarian¹, Anne Dell³,
Michael Demetriou^{1,2*}

¹Department of Microbiology and Molecular Genetics, University of California, Irvine, United States; ²Department of Neurology and Institute for Immunology, University of California, Irvine, United States; ³Department of Life Sciences, Imperial College London, London, United Kingdom

Abstract Essential biological systems employ self-correcting mechanisms to maintain cellular homeostasis. Mammalian cell function is dynamically regulated by the interaction of cell surface galectins with branched N-glycans. Here we report that N-glycan branching deficiency triggers the Golgi to generate bioequivalent N-glycans that preserve galectin-glycoprotein interactions and cellular homeostasis. Galectins bind N-acetylglucosamine (LacNAc) units within N-glycans initiated from UDP-GlcNAc by the *medial*-Golgi branching enzymes as well as the *trans*-Golgi poly-LacNAc extension enzyme β 1,3-N-acetylglucosaminyltransferase (B3GNT). Marginally reducing LacNAc content by limiting N-glycans to three branches results in T-cell hyperactivity and autoimmunity; yet further restricting branching does not produce a more hyperactive state. Rather, new poly-LacNAc extension by B3GNT maintains galectin binding and immune homeostasis. Poly-LacNAc extension is triggered by redistribution of unused UDP-GlcNAc from the *medial* to *trans*-Golgi via inter-cisternal tubules. These data demonstrate the functional equivalency of structurally dissimilar N-glycans and suggest a self-correcting feature of the Golgi that sustains cellular homeostasis.

DOI: 10.7554/eLife.14814.001

*For correspondence: mdemetri@uci.edu

Competing interests: The authors declare that no competing interests exist.

Funding: See page 23

Received: 29 January 2016

Accepted: 07 June 2016

Published: 08 June 2016

Reviewing editor: Benjamin S Glick, The University of Chicago, United States

© Copyright Mkhikian et al. This article is distributed under the terms of the [Creative Commons Attribution License](#), which permits unrestricted use and redistribution provided that the original author and source are credited.

Introduction

Self-correcting mechanisms have evolved to maintain the integrity of critical biological pathways in the face of disruptive insults and stochastic uncertainty. Such mechanisms range from proofreading in DNA replication to functional redundancy of important cellular apparatuses. The galectin-glycoprotein lattice is a dynamic cell surface structure that globally regulates receptor localization and signaling (Demetriou et al., 2001; Partridge et al., 2004; Lau et al., 2007; Dennis et al., 2009; Grigorian et al., 2009). Its importance is underscored by its role in basic cellular processes such as signaling, apoptosis, endocytosis, differentiation, and cell growth, as well as its association with a wide range of diseases including immunity/autoimmunity (Demetriou et al., 2001; Lee et al., 2007; Mkhikian et al., 2011; Li et al., 2013; Wang et al., 2015; Zhou, 2014), cancer (Dennis et al., 1987; Fernandes et al., 1991; Granovsky et al., 2000; Beheshti Zavareh et al., 2012; Croci et al., 2014), and Type 2 diabetes (Ohtsubo et al., 2005; Johswich et al., 2014). However, a mechanism that homeostatically sustains the lattice is not known.

The lattice forms due to the multivalent interactions between extracellular galectins, a family of sugar binding proteins, and the disaccharide N-acetylglucosamine (LacNAc) present on Asn (N)-linked glycans attached to cell surface glycoproteins (Hirabayashi et al., 2002; Brewer et al., 2002; Ahmad et al., 2004). The vast majority of secreted and cell surface proteins are co- or post-

eLife digest Most proteins that are released from cells are modified with sugar molecules that allow the proteins to carry out their role properly. These modifications are called glycans, and are made from sugar subunits joined into chains or branched structures. Investigating how the structure of glycans is linked to their role is complicated by the fact that many different glycans exist, made up of different sugars and arranged into different structures.

Enzymes located in cell compartments known as the endoplasmic reticulum and the Golgi help to build the glycans. For example, the MGAT family of enzymes found in the Golgi generates branched glycans made up of sugar subunits called N-acetylglucosamine (GlcNAc). These glycans form part of a molecular mesh on the surface of cells that controls how certain proteins embedded in the cell membrane behave. This is particularly important in immune cells: reducing the number of branches in the glycans weakens the mesh and causes the cells and their membrane proteins to behave inappropriately.

Mkhikian et al. have studied mice that lack specific MGAT enzymes, and so produce LacNAc glycans with drastically fewer branches than normal. Immune cells in these mice had glycans on their surface formed of LacNAc arranged in chains, rather than in short branched structures. These chains turned out to be biologically equivalent to branched LacNAc glycans, containing the same sugar subunits and allowing the immune cells to behave as normal. This suggests that the composition of glycans, rather than their structure, primarily determines their role.

Mkhikian et al. also found that the organization of the enzymes inside the Golgi is likely to be responsible for producing these equivalent glycans. A glycan is built up as it passes through the Golgi, with the branching enzymes located earlier in the Golgi than the extending enzymes. Therefore, if the branching enzymes fail to add LacNAc subunits to the glycan, the extending enzymes can step in later to add the missing components.

Overall, the results presented by Mkhikian et al. indicate that the large number of structurally diverse glycans may be reduced to a much smaller number of glycans with similar roles, based on subunit composition. This will simplify future studies on LacNAc glycans, and further work could focus on defining which other glycan structures share similar roles.

DOI: [10.7554/eLife.14814.002](https://doi.org/10.7554/eLife.14814.002)

translationally modified by the addition of sugars in the ER. As these proteins transit through the ER and Golgi, their glycans undergo dramatic remodeling, generating a vast and heterogeneous array of glycoforms (*Kornfeld and Kornfeld, 1985; Schachter, 1991*). In the *medial* Golgi a group of enzymes, MGAT1, 2, 4, and 5, act to produce N-glycans with one, two, three, or four N-acetylglucosamine (GlcNAc) branches (*Schachter, 1986*). The subsequent addition of galactose by a family of galactosyl transferase enzymes produces the galectin substrate LacNAc (*Figure 1—figure supplement 1A*). The number of branches depends on the relative activity of the *medial* Golgi branching enzymes MGAT1, 2, 4, and 5 and the availability of their shared donor substrate UDP-GlcNAc (*Lau et al., 2007; Dennis et al., 2009; Grigorian et al., 2007; 2011*). Alternating action of β 1,3-N-acetylglucosaminyltransferase (B3GNT) and galactosyl transferase enzymes can generate a linear polymer of LacNAc (poly-LacNAc) at any given branch. Although the affinity of galectin binding to a LacNAc monomer is relatively weak, increased LacNAc valency through branching and poly-LacNAc extension can dramatically increase galectin avidity leading to a major impact on cell surface dynamics (*Hirabayashi et al., 2002*). In T cells for example, galectin - T cell receptor (TCR) interactions directly oppose ligand induced TCR clustering and signaling, thereby negatively regulating T cell development, antigen-dependent T cell growth, and autoimmunity risk.

Glycan analysis of tissues from glycosylation pathway deficient mice has revealed the presence of minor but unusual structures (*Stone et al., 2009; Takamatsu et al., 2010; Ismail et al., 2011*). The function of these changes is unclear, but some have suggested that the observed structural alterations may reflect production of bioequivalent glycans that are induced by communication between the cell surface and the Golgi (*Takamatsu et al., 2010; Dam and Brewer, 2010; Dennis and Brewer, 2013*). However, direct evidence supporting this possibility is lacking. Deficiency in the branching enzyme β 1,6-N-acetylglucosaminyltransferase V (MGAT5) reduces avidity for galectin,

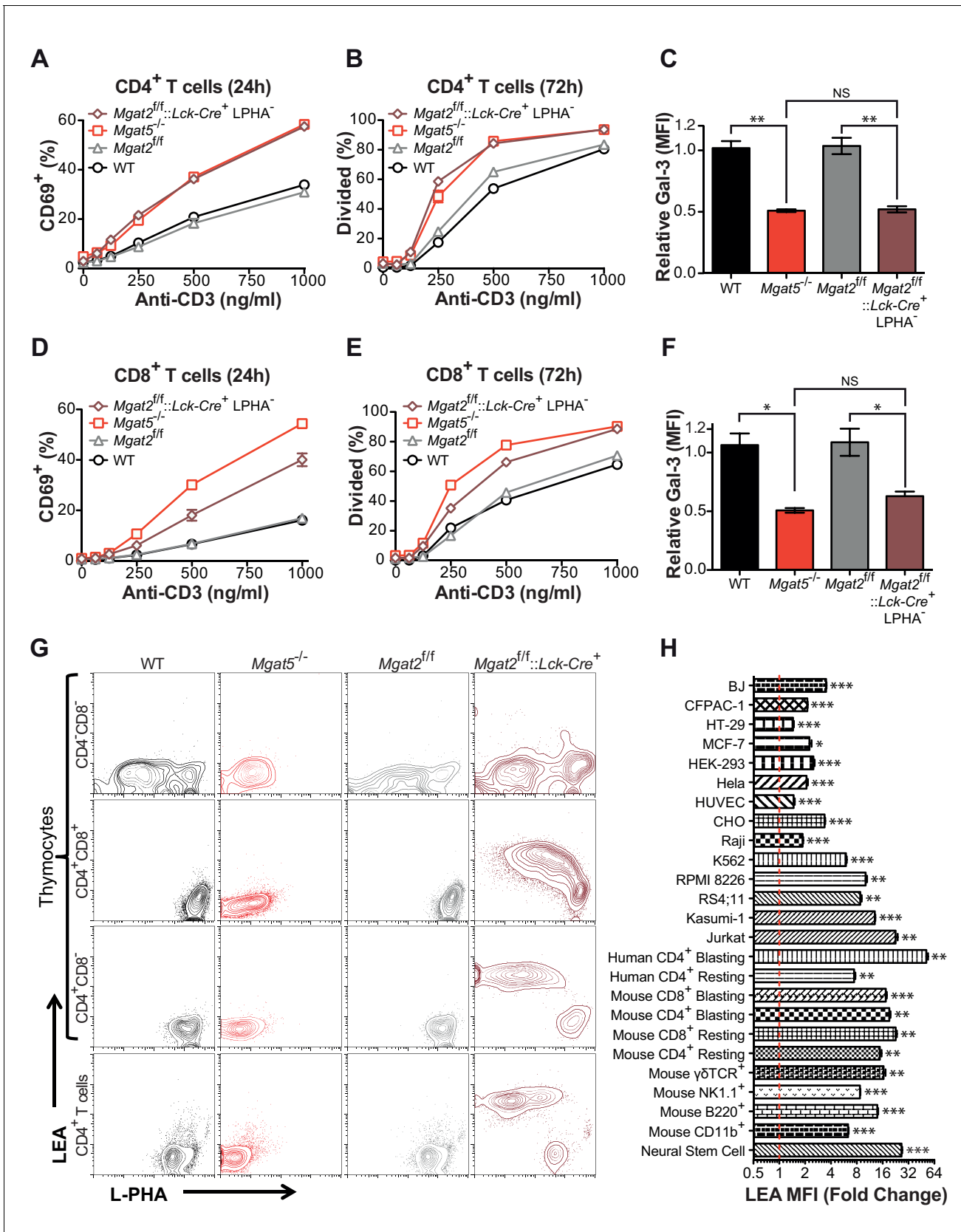


Figure 1. Compensation limits hyperactivity of *Mgat2* deficient T cells. (A, B, D and E) T cells were activated with plate bound anti-CD3 for 24 (A and D) or 72 (B and E) hours. CD4⁺ (A and B) or CD8⁺ (D and E) cells were analyzed for CD69 expression (A and D) or 5, 6-carboxyfluorescein diacetate
 Figure 1 continued on next page

Figure 1 continued

succinimidyl ester (CFSE) dilution (B and E) by flow cytometry, gating on L-PHA⁻ cells where indicated. (C and F) T cells were analyzed for galectin-3 binding by flow cytometry, gating on CD4⁺ (C) or CD8⁺ (F) cells and L-PHA⁻ cells where indicated. Normalized geometric mean fluorescence intensity (MFI) is shown. Each mutant was normalized to its control. (G) Thymocytes and splenic T cells were analyzed for L-PHA and LEA binding by flow cytometry. (H) Cells were treated in culture with or without 500 nM SW for 72 hr followed by analysis of LEA binding by flow cytometry. Fold increase in LEA MFI of the SW treated sample compared to the untreated sample is presented. The red line marks one fold or no change. NS, not significant; *p<0.05; **p<0.01; ***p<0.001 (unpaired two-tailed t-test with Welch's (C, F and H) and Bonferroni correction (C and F)). Data show one experiment representative of at least three independent experiments. Error bars indicate mean ± s.e.m.

DOI: 10.7554/eLife.14814.003

The following figure supplement is available for figure 1:

Figure supplement 1. The hexosamine and N-glycan biosynthetic pathways in mammals.

DOI: 10.7554/eLife.14814.004

enhancing antigen dependent and independent TCR clustering/signaling, leading to development of spontaneous autoimmune disease (Demetriou et al., 2001; Lee et al., 2007). Based on the current model of the galectin-glycoprotein lattice, more severe reductions in branching should weaken the lattice further and result in greater T cell hyperactivity. Surprisingly, further limiting branching revealed that the Golgi apparatus has a remarkable capacity to buffer challenges to the strength of the galectin-glycoprotein lattice. Our analysis reveals a homeostatic mechanism built into the architecture of the Golgi apparatus that induces bioequivalent poly-LacNAc glycans that act to maintain the function of the galectin-glycoprotein lattice in the face of dysregulated Golgi branching.

Results

Mgat2 deficiency does not increase T cell hyperactivity beyond Mgat5 deficiency

To further investigate the role of branching in T cells, we generated T cell specific *Mgat2* deficient mice (*Mgat2^{fl/fl}::Lck-Cre⁺*) (Ye and Marth, 2004). Loss of *Mgat2* is expected to limit N-glycans to a single branch, producing hybrid structures; although a second branch via MGAT4 activity is possible (Figure 1—figure supplement 1A). As the branching pathway declines in enzymatic efficiency going from MGAT1 to MGAT5, *Mgat2* deficiency also impacts a much greater percentage of cell surface glycans than *Mgat5* deletion (Wang et al., 2001). Examination of peripheral T cells from *Mgat2^{fl/fl}::Lck-Cre⁺* mice indicated loss of *Mgat2* in most but not all T cells as assayed by flow cytometry with the plant lectin L-PHA (*Phaseolus vulgaris*, leucoagglutinin) (Figure 1—figure supplement 1B). β1,6GlcNAc-branched N-glycans produced by MGAT5 specifically bind L-PHA, structures that are also lost following *Mgat2* deletion (Demetriou et al., 2001; Cummings and Kornfeld, 1982). Surprisingly, *Mgat5* and *Mgat2* deficient CD4⁺ and CD8⁺ T cells displayed a similar degree of activation and proliferation in response to anti-CD3 (an antibody which induces TCR clustering and signaling) despite the more dramatic reduction in LacNAc branching in *Mgat2* deficient T cells (Figure 1A,B,D and E). This suggested that either the β1,6GlcNAc branch produced by the MGAT5 enzyme is uniquely important for regulating T cell activation or that a compensatory mechanism maintains galectin binding when the number of LacNAc branches is reduced. To evaluate for potential differences in total surface LacNAc content between *Mgat2* and *Mgat5* deficient T cells, galectin-3 binding at the cell surface was measured by flow cytometry. *Mgat5* deletion resulted in a significant reduction in the ability of CD4⁺ and CD8⁺ T cells to bind galectin-3 (Figure 1C and F), consistent with previously published results (Demetriou et al., 2001). However, *Mgat2* deficiency produced no additional decrease in galectin-3 binding (Figure 1C and F), suggesting comparable LacNAc content at the cell surface despite a marked reduction in LacNAc branches in *Mgat2* relative to *Mgat5* deficient T cells.

Inhibition of LacNAc branching results in linear extension with poly-LacNAc

Since the branching pathway enzymes act sequentially, we hypothesized that compensatory maintenance of cell surface LacNAc content in *Mgat2* deficient T cells would primarily occur by poly-LacNAc extension of the MGAT1 generated branch (Figure 1—figure supplement 1A). To test this

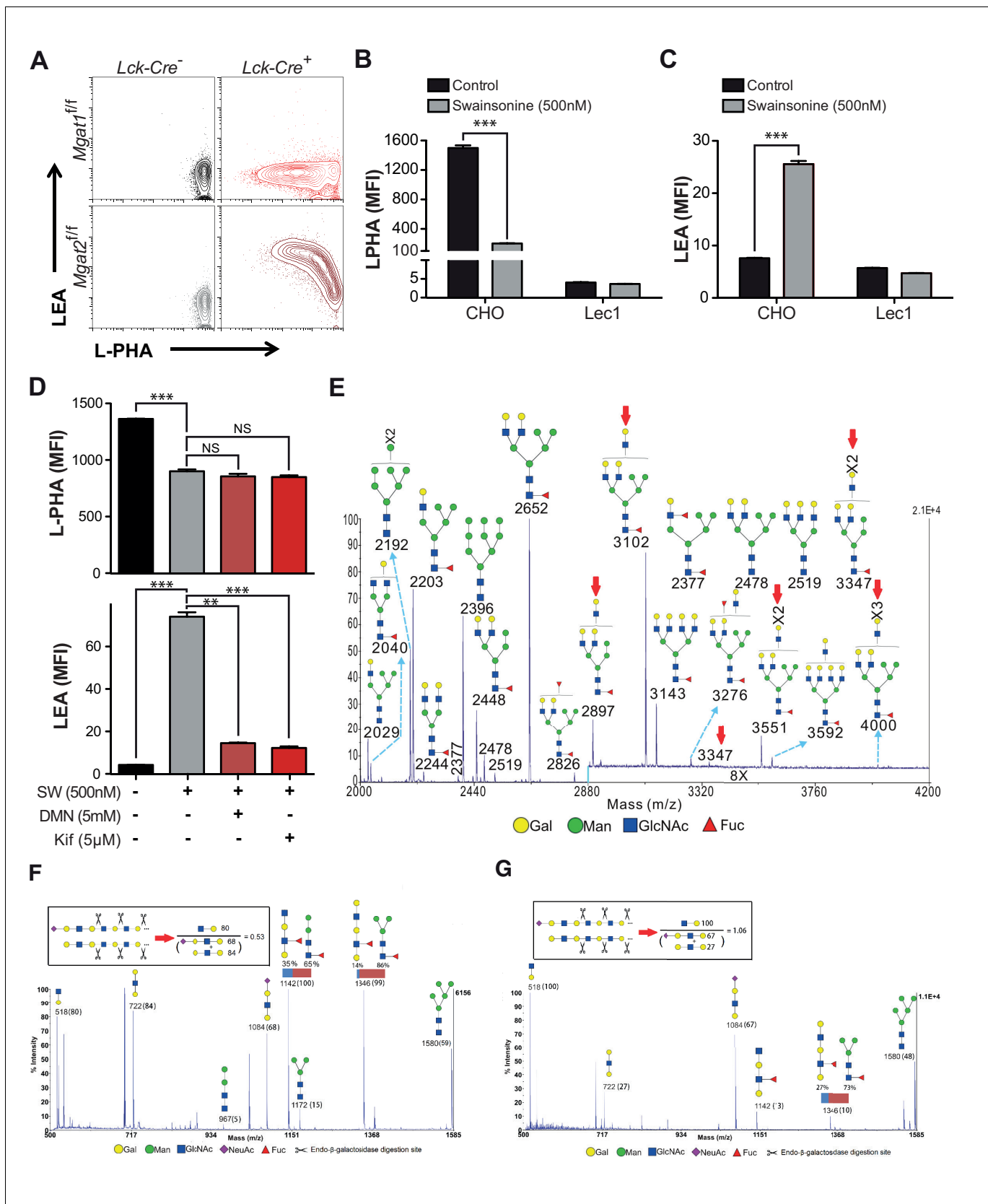


Figure 2. Branching deficiency induces poly-LacNAc on N-glycans. (A) Thymocytes were analyzed for L-PHA and LEA binding by flow cytometry, gating on CD4⁺CD8⁺ double positive cells. (B and C) CHO and Lec1 cells were grown in the presence or absence of 500 nM SW for 3 days followed by

Figure 2 continued on next page

Figure 2 continued

analysis for L-PHA (B) or LEA (C) binding by flow cytometry. (D) Resting primary human T cells were treated as indicated for 3 days and analyzed for L-PHA (upper) or LEA (lower) binding by flow cytometry, gating on live, non-blasting CD4⁺ cells. (E–G) MALDI-TOF analysis of Sialidase A (E) or Endo- β -galactosidase treated N-glycans from Jurkat T cells treated without (F) or with SW (E and G). Hybrid glycans with extended antennae were observed in (E) at m/z 2897, 3102, 3347, 3551 and 4000, which are highlighted with red arrows. The % intensities of the peaks in (F, G) are shown in the brackets after m/z values. The signals at m/z 518, 722 and 1084 are derived from linear poly-LacNAc antennae and are used to represent the length of antennae. The calculation is shown above the spectrum. In addition, a minority of non-sialylated poly-LacNAc antennae were found to be internally fucosylated yielding GlcNAc β 1,3Gal β 1,4(Fuc α 1,3)GlcNAc β 1,3Gal (m/z 1142) and Gal β 1,4GlcNAc β 1,3Gal β 1,4(Fuc α 1,3)GlcNAc β 1,3Gal (m/z 1346) upon digestion. MS/MS analysis of the peaks at m/z 1142 and 1346 also revealed the presence of isobaric pauci-mannose glycans, their relative abundances are indicated on the figure (see **Figure 2—figure supplement 3**). Ions are in the form of M⁺Na⁺. Peaks are annotated with putative structures according to the molecular weight, the glycan biosynthetic pathway and for (E), the MALDI-TOF analysis of the N-glycans before Sialidase A treatment (shown in **Figure 2—figure supplement 2**). NS, not significant; **p<0.01; ***p<0.001 (unpaired two-tailed t-test with Welch's (B–D) and Bonferroni correction (D)). Data show one experiment representative of at least three independent experiments (A–D), except mass spectrometry (E–G), which was performed once. Error bars indicate mean \pm s.e.m.

DOI: [10.7554/eLife.14814.005](https://doi.org/10.7554/eLife.14814.005)

The following figure supplements are available for figure 2:

Figure supplement 1. Induction of poly-LacNAc structures occurs preferentially on N-glycans.

DOI: [10.7554/eLife.14814.006](https://doi.org/10.7554/eLife.14814.006)

Figure supplement 2. MALDI-TOF analysis of N-glycans from SW treated Jurkat T cells MALDI-TOF analysis of N-glycans from SW treated Jurkat T cells.

DOI: [10.7554/eLife.14814.007](https://doi.org/10.7554/eLife.14814.007)

Figure supplement 3. MS/MS analysis of endo- β -galactosidase digested glycans from Jurkat T cells.

DOI: [10.7554/eLife.14814.008](https://doi.org/10.7554/eLife.14814.008)

prediction, T cells and thymocytes were stained with L-PHA as well as the *Lycopersicon Esculentum* lectin (LEA). LEA binds to poly-LacNAc structures containing at least three repeating LacNAc units (Kawashima et al., 1990; Merkle and Cummings, 1987). Wild type and *Mgat5*^{-/-} T cells and thymocytes expressed very low levels of poly-LacNAc. However, in *Mgat2*^{ff/ff}::*Lck-Cre*⁺ mice, loss of L-PHA staining was accompanied by a ~100 fold increase in LEA staining. The loss of L-PHA binding and the increase in LEA binding appeared to occur concurrently during the double positive stage of thymocyte development, shortly after the *Lck* promoter driven *Cre* is first expressed, and were maintained through the single positive stage and in peripheral T cells (Figure 1G). Treatment of various cell types with swainsonine (SW), a mannosidase II inhibitor which blocks N-glycan processing between MGAT1 and MGAT2 (Figure 1—figure supplement 1A), indicated that homeostatic up-regulation of poly-LacNAc was a general feature of many cell types including epithelial, mesenchymal, and hematopoietic cells; with the greatest responses in the latter (Figure 1H).

Poly-LacNAc may occur on N-glycans as well as O-glycans and glycolipids (Fukuda et al., 1986; Watanabe et al., 1979). Furthermore, LEA has been reported to bind to high-mannose structures in addition to poly-LacNAc (Oguri, 2005). To investigate the structural basis for the increase in LEA staining, *Mgat2* deficient T cells were treated with PNGase F, an amidase which specifically cleaves N-glycans (Maley et al., 1989). PNGase F treatment of live cells incompletely removes N-glycans, with a four hour treatment of *Mgat2*^{ff/ff} T cells reducing cell surface L-PHA binding by ~50% (Figure 2—figure supplement 1A–B). Nevertheless, the same treatment resulted in a >80% reduction in LEA binding in *Mgat2* deficient T cells, suggesting that the vast majority of LEA staining was due to cell surface N-glycans (Figure 2—figure supplement 1C–D). To further evaluate this question, we directly compared thymocytes derived from *Mgat2*^{ff/ff}::*Lck-Cre*⁺ and *Mgat1*^{ff/ff}::*Lck-Cre*⁺ mice (Zhou, 2014). *Mgat1* deficiency blocks all branching and poly-LacNAc extension in N-glycans, but not O-glycans or glycolipids. Indeed, unlike *Mgat2* deficiency, *Mgat1* deficient thymocytes do not show an increase in LEA staining concurrent with the loss in L-PHA staining (Figure 2A). Similarly, SW increases LEA staining in CHO cells but not *Mgat1* deficient CHO (Lec1) cells (Figure 2B and C). Furthermore, increased LEA staining induced by SW treatment of T cells was reversed by the mannosidase I inhibitors deoxymannojirimycin (DMN) and kifunensine (kif), which block the N-glycan pathway prior to MGAT1 (Figure 2D).

Poly-LacNAc content was also investigated using mass spectrometric glycomic methodologies. SW treated Jurkat cells, rather than T cells from *Mgat2*^{ff/ff}::*Lck-Cre*⁺ mice, were used for this purpose to provide a sufficient amount of starting material for accurate analysis. MALDI-TOF-MS of N-glycans

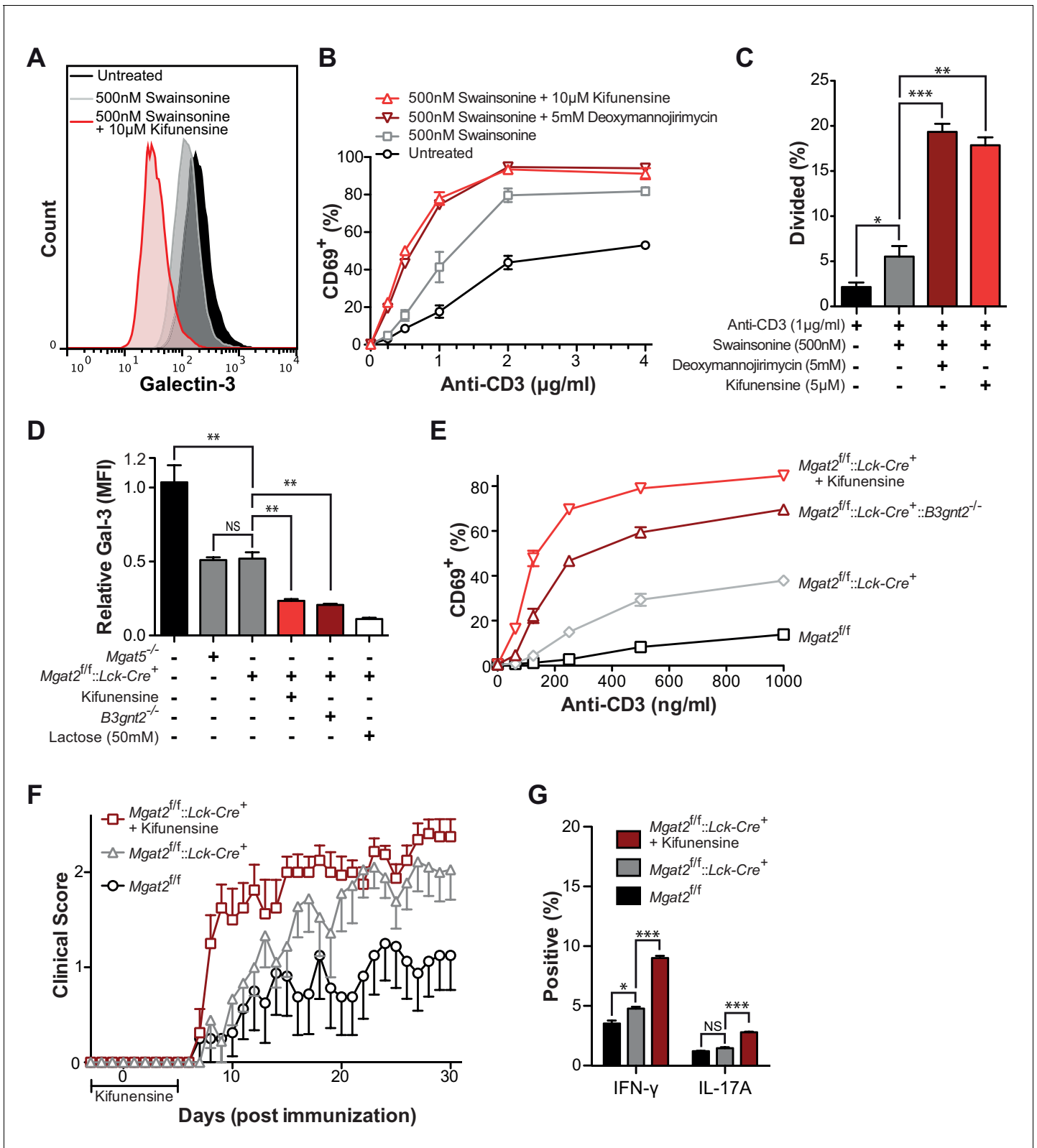


Figure 3. Poly-LacNAc compensation opposes T cell activation and autoimmunity. (A) Jurkat T cells were treated as indicated for 72 hr in culture and analyzed for galectin-3 binding by flow cytometry. (B and C) Human T cells were pre-treated as indicated for 72 hr in culture without stimulation, then activated with plate bound anti-CD3 for 24 (B) or 72 (C) hours and analyzed for CD69 expression (B) or CFSE dilution (C) by flow cytometry, gating on CD4⁺ cells. (D) Mouse T cells were analyzed for galectin-3 binding by flow cytometry, gating on CD4⁺ cells. Where indicated, mice were pre-treated for 24 hr with lactose. (E) Mouse T cells were analyzed for CD69 expression by flow cytometry, gating on CD4⁺ cells. (F) Mice were immunized with anti-CD3 and analyzed for clinical scores over time. (G) Mice were immunized with anti-CD3 and analyzed for IFN-γ and IL-17A production by flow cytometry, gating on CD4⁺ cells. Statistical significance is indicated by asterisks (*p < 0.05, **p < 0.01, ***p < 0.001) or NS (not significant).

Figure 3 continued

3 days with 0.2 mg/ml kifunensine in the drinking water. (E) Mouse T cells were activated for 24 hr with plate bound anti-CD3 and analyzed for CD69 expression by flow cytometry, gating on CD4⁺ cells. Where indicated, mice were pre-treated for 3 days with 0.2 mg/ml kifunensine in the drinking water followed by 10 μ M kifunensine during culture. (F) EAE was induced in age matched female C57BL/6 mice treated with or without kifunensine in the drinking water at 0.2 mg/ml from day -3 to 5, with day 0 indicating the time of immunization (n = 9 per group). (G) On day 30, splenocytes were isolated from representative mice of each EAE group and analyzed for cytokine expression by flow cytometry. NS, not significant; *p<0.05; **p<0.01; ***p<0.001 (unpaired two-tailed t-test with Welch's (C, D and G) and Bonferroni correction (C, D and G)). Data shown are one experiment representative of at least three independent experiments (A–E), except EAE (F and G), which was performed once. Error bars indicate mean \pm s.e.m.

DOI: [10.7554/eLife.14814.009](https://doi.org/10.7554/eLife.14814.009)

The following figure supplement is available for figure 3:

Figure supplement 1. Poly-LacNAc compensation opposes T cell activation and autoimmunity.

DOI: [10.7554/eLife.14814.010](https://doi.org/10.7554/eLife.14814.010)

derived from SW treated Jurkat T cells confirmed the presence of hybrid N-glycans with up to two poly-LacNAc extended branches (m/z 2897, 3102, 3347, 3551, and 4000 in **Figure 2E**, **Figure 2—figure supplement 2**). This was qualitatively consistent with the presence of poly-LacNAc following SW treatment, but likely under-represents the length of poly-LacNAc extension due to the limited sensitivity of MALDI-TOF-MS for large poly-LacNAc structures. To better quantitate the change in poly-LacNAc, endo- β -galactosidase digestion was used. This enzyme cuts all internal Gal β 1,4 linkages in poly-LacNAc structures, unless the GlcNAc on its reducing side is modified by fucose. Endo- β -galactosidase digestion produced GlcNAc β 1,3Gal (m/z 518) from internal linear poly-LacNAc antennae, together with Gal β 1,4GlcNAc β 1,3Gal (m/z 722) and NeuAc-Gal β 1,4GlcNAc β 1,3Gal (m/z 1084) from their non-reducing termini (**Figure 2F,G** and **Figure 2—figure supplement 3**). The ratio of the internal and terminal glycans examines the relative length of linear poly-LacNAc structures, with a higher ratio signifying longer chains. The non-treated cells had a ratio of 0.5, which increased to 1.1 in the SW treated cells (**Figure 2F and G**), confirming the presence of longer poly-LacNAc chains after SW treatment. *Mgat2* deficient T cells are expected to have a greater increase, given the ~100 fold increase in LEA binding compared to the ~20 fold increase in SW treated Jurkat cells. Together, these data indicate that severe LacNAc branching deficiency increases poly-LacNAc structures on N-glycans.

Homeostatic poly-LacNAc opposes T cell hyperactivity and autoimmunity

To assess the functional consequences of poly-LacNAc up-regulation, we first reversed SW induced poly-LacNAc by blocking all branching using the mannosidase I inhibitors deoxymannojirimycin (DMN) or kifunensine. Whereas SW treatment alone moderately reduced galectin-3 binding, the addition of kifunensine dramatically reduced galectin-3 binding of Jurkat T cells (**Figure 3A**). As previously shown, SW treatment alone caused significant increases in both anti-CD3 induced activation and proliferation of primary human T cells (**Figure 3B,C** and **Figure 3—figure supplement 1**). However, the addition of kifunensine or DMN resulted in much greater hyperactivity, particularly at lower doses of anti-CD3. Careful titration of kifunensine in the presence of SW did not further reduce L-PHA binding, yet caused a dose dependent decrease in LEA binding and increase in CD69 induction, indicating that poly-LacNAc extension dose dependently regulates T cell activation thresholds (**Figure 3—figure supplement 1A–B**).

To further confirm the functional role of homeostatic induction of poly-LacNAc, mouse T cells deficient in both *Mgat2* and *B3gnt2* were generated. B3GNT2 is one of the major B3GNT enzymes responsible for poly-LacNAc branch extension in mouse T cells and poly-LacNAc up-regulation is expected to be limited in its absence (*Togayachi et al., 2007*). Indeed, T cells from *Mgat2*^{fl/fl}::*Lck-Cre*⁺::*B3gnt2*^{-/-} mice showed significantly reduced galectin-3 binding when compared to *Mgat2* deficient T cells, confirming reduced LacNAc content (**Figure 3D**). Directly comparing T cell activation between these lines showed that both genetic and pharmacological inhibition of homeostatic poly-LacNAc extension resulted in significantly increased T cell hyperactivity (**Figure 3E**).

Since the galectin lattice has been shown to inhibit autoimmunity, we next sought to determine the functional consequences of glycomic homeostasis in regulating the course and severity of experimental autoimmune encephalomyelitis (EAE), a model that mimics the autoimmune CNS pathology

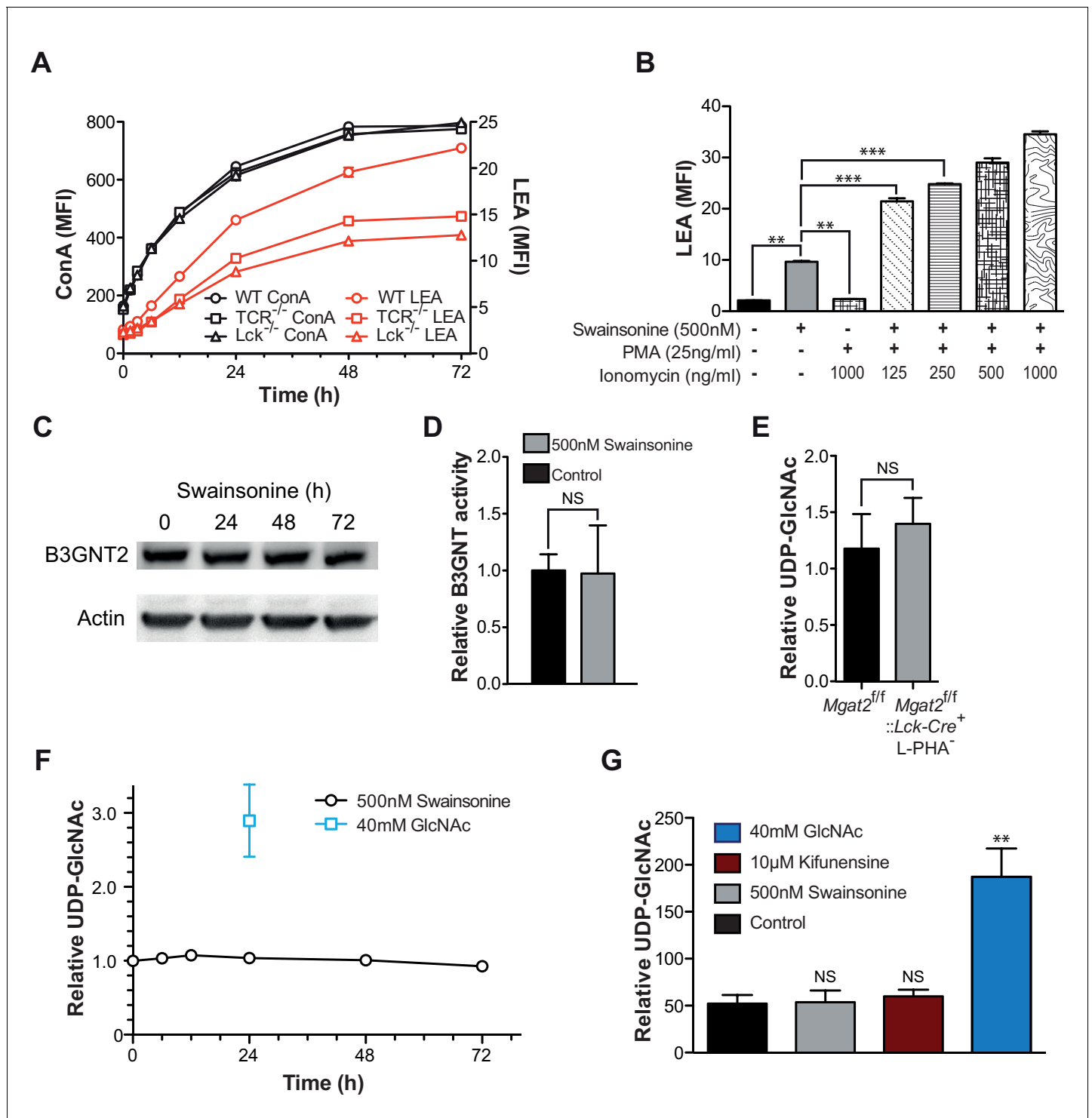


Figure 4. Increased TCR signaling and UDP-GlcNAc levels are neither necessary nor sufficient for poly-LacNAc induction. (A) WT, TCR $\beta^{-/-}$ and Lck $^{-/-}$ Jurkat cells were treated with SW for the indicated times and analyzed for lectin binding by flow cytometry. (B) Jurkat cells were treated as indicated for 24 hr and analyzed for LEA binding by flow cytometry. (C) Lysates of Jurkat T cells treated with SW as indicated were immune-blotted with anti-B3GNT2 and actin. (D) B3GNT enzyme activity was measured in lysates of Jurkat T cells treated with and without SW for 72 hr. (E–G) Total cellular UDP-GlcNAc levels were measured in mouse T cells (E), or Jurkat T cells treated as indicated (F, G) via mass spectrometry (E and G) or a spectrophotometric method (F). Jurkat cells were treated for the indicated times (F) or for 24 hr (G). NS, not significant; * $p < 0.05$; ** $p < 0.01$; *** $p < 0.001$ (unpaired two-tailed t-test with Welch's (B, D, E and G) and Bonferroni correction (B and G)). Data show one experiment representative of at least three independent experiments. Error bars indicate mean \pm s.e.m.

Figure 4 continued on next page

Figure 4 continued

DOI: [10.7554/eLife.14814.011](https://doi.org/10.7554/eLife.14814.011)

The following figure supplement is available for figure 4:

Figure supplement 1. TCR signaling and cellular UDP-GlcNAc levels modulate the degree of poly-LacNAc induced by branching Deficiency.

DOI: [10.7554/eLife.14814.012](https://doi.org/10.7554/eLife.14814.012)

of multiple sclerosis (*Grigorian et al., 2011*). *Mgat2^{ff}* and *Mgat2^{ff}::Lck-Cre⁺* mice were treated with either vehicle or kifunensine in the drinking water from day -3 to 5, with day 0 indicating time of immunization. As expected, vehicle treated *Mgat2^{ff}::Lck-Cre⁺* mice displayed a significantly more severe EAE than vehicle treated *Mgat2^{ff}* mice. However, kifunensine treatment of *Mgat2^{ff}::Lck-Cre⁺* mice resulted in a dramatic increase in clinical score and disease incidence early in the disease course, a difference that narrowed later in the absence of kifunensine (*Figure 3F* and *Figure 3—supplement figure 1D*). Kifunensine treated mice also had more pro-inflammatory T_H1 and T_H17 cells compared to vehicle treated mice *in vivo* and following re-stimulation with MOG 35–55 *in vitro* (*Figure 3G*, *Figure 3—figure supplement 1E*). Taken together these data demonstrate a major role for homeostatic poly-LacNAc extension in controlling T cell growth, differentiation, and self-tolerance.

Homeostatic poly-LacNAc is not induced by alterations in enzyme activity

As the galectin-glycoprotein lattice negatively regulates TCR signaling and TCR signaling promotes lattice strength (*Demetriou et al., 2001*; *Chen et al., 2009*), we hypothesized that LacNAc homeostasis may result from a feedback loop linking TCR signaling and cell surface LacNAc content. Such a mechanism, which depends on a cell surface sensor of Golgi activity/branching implies a temporal lag phase during which a defect is detected, a signal is sent, and then the Golgi generates the proper response. With this prediction in mind, Jurkat T cells were treated with SW for various times and analyzed for changes in cell surface glycosylation by L-PHA, LEA, and Concanavalin A (ConA), the latter a plant lectin that binds high-mannose structures increased by SW treatment (*Figure 4—figure supplement 1A–C*). Although the increase in LEA binding trailed slightly behind an increase in ConA binding, it began to increase within ~1.5 hr of SW treatment, indicating an almost immediate compensatory response. Loss of L-PHA staining exhibited the smallest slope, possibly reflecting the preferential cell surface retention of highly branched glycoproteins (*Figure 4—figure supplement 1C*).

Since the increase in LEA staining exhibited some delay, the role of TCR signaling in driving poly-LacNAc induction was assessed. Blocking TCR signaling genetically, with TCR β and Lck deficient Jurkat lines, or pharmacologically, with MAP kinase inhibitors, only partially reduced the magnitude of the poly-LacNAc response induced by SW (*Figure 4A* and *Figure 4—figure supplement 1D*). More importantly, directly activating downstream TCR signaling with PMA and ionomycin did not induce poly-LacNAc up-regulation, although it further enhanced poly-LacNAc triggered by SW (*Figure 4B*). Thus, TCR signaling appears to be neither necessary nor sufficient for the homeostatic poly-LacNAc response, but does contribute to its magnitude in the context of deficient branching.

Since most surface receptors are glycosylated, there are a large number of possible additional cell surface sensors that may alter signaling to drive compensation. However, we reasoned that regardless of the upstream components, a mechanism that acts to increase poly-LacNAc production must do so by either increasing the activity of responsible enzymes or increasing substrate supply (UDP-GlcNAc or glycoprotein) for the reaction. It is unlikely that an increase in mono-antennary glycans could account for the observed compensatory response, as all branches are equally likely to be extended with poly-LacNAc (*Antonopoulos et al., 2012*; *Ishida et al., 2005*).

Microarray analysis of purified *Mgat2^{+/+}* and *Mgat2^{-/-}* CD4⁺ T cells revealed no significant changes in glycosylation genes known to impact poly-LacNAc production or UDP-GlcNAc biosynthesis (*Table 1*). Gene expression was altered in some genes unrelated to glycosylation, but these are likely related to downstream effects of *Mgat2* deficiency (*Table 2*). Comparing B3GNT2 protein levels in Jurkat T cells treated with or without SW also showed no difference (*Figure 4C*). Total poly-LacNAc enzyme activity in lysates from control and SW treated Jurkat T cells also revealed no

Table 1. List of N-glycan branching, poly-LacNAc production, and hexosamine pathway genes.

Gene symbol	Gene description	p Value	Fold change
Man1a	mannosidase 1, alpha	0.3602	1.0628
Man1a2	mannosidase, alpha, class 1A, member 2	0.4885	-1.0551
Man1b1	mannosidase, alpha, class 1B, member 1	0.4397	-1.0627
Man1c1	mannosidase, alpha, class 1C, member 1	0.4053	1.0748
Man2a1	mannosidase 2, alpha 1	0.8150	-1.0168
Man2a2	mannosidase 2, alpha 2	0.3647	-1.0787
Man2b1	mannosidase 2, alpha B1	0.0800	-1.1350
Man2b2	mannosidase 2, alpha B2	0.6465	1.0331
Man2c1	mannosidase, alpha, class 2C, member 1	0.9826	1.0016
Mgat1	mannoside acetylglucosaminyltransferase 1	0.1005	-1.1846
Mgat2	mannoside acetylglucosaminyltransferase 2	0.0000	-27.8780
Mgat3	mannoside acetylglucosaminyltransferase 3	0.1757	1.1377
Mgat4a	mannoside acetylglucosaminyltransferase 4, isoenzyme A	0.1486	-1.2068
Mgat4b	mannoside acetylglucosaminyltransferase 4, isoenzyme B	0.2248	1.1345
Mgat4c	mannosyl (alpha-1,3-)-glycoprotein beta-1,4-N-acetylglucosaminyltransferase, isozyme C (putative)	0.5695	1.0539
Mgat5	mannoside acetylglucosaminyltransferase 5	0.4045	1.0666
Mgat5b	mannoside acetylglucosaminyltransferase 5, isoenzyme B	0.1450	1.1347
B3gnt1	UDP-GlcNAc:betaGal beta-1,3-N-acetylglucosaminyltransferase 1	0.5597	-1.0587
B3gnt2	UDP-GlcNAc:betaGal beta-1,3-N-acetylglucosaminyltransferase 2	0.1503	1.1219
B3gnt3	UDP-GlcNAc:betaGal beta-1,3-N-acetylglucosaminyltransferase 3	0.4031	1.1072
B3gnt4	UDP-GlcNAc:betaGal beta-1,3-N-acetylglucosaminyltransferase 4	0.2923	1.1100
B3gnt5	UDP-GlcNAc:betaGal beta-1,3-N-acetylglucosaminyltransferase 5	0.1758	1.1742
B3gnt6	UDP-GlcNAc:betaGal beta-1,3-N-acetylglucosaminyltransferase 6 (core 3 synthase)	0.5565	1.0511
B3gnt7	UDP-GlcNAc:betaGal beta-1,3-N-acetylglucosaminyltransferase 7	0.8028	1.0237
B3gnt8	UDP-GlcNAc:betaGal beta-1,3-N-acetylglucosaminyltransferase 8	0.6157	1.0443
B3gnt9-ps	UDP-GlcNAc:betaGal beta-1,3-N-acetylglucosaminyltransferase 9, pseudogene	0.2841	1.0856
B3gnt11	UDP-GlcNAc:betaGal beta-1,3-N-acetylglucosaminyltransferase-like 1	0.7979	-1.0241
B4galt1	UDP-Gal:betaGlcNAc beta 1,4- galactosyltransferase, polypeptide 1	0.8003	1.0166
B4galt2	UDP-Gal:betaGlcNAc beta 1,4- galactosyltransferase, polypeptide 2	0.1023	1.1487
B4galt3	UDP-Gal:betaGlcNAc beta 1,4-galactosyltransferase, polypeptide 3	0.6938	-1.0304
B4galt4	UDP-Gal:betaGlcNAc beta 1,4-galactosyltransferase, polypeptide 4	0.1378	1.1624
B4galt5	UDP-Gal:betaGlcNAc beta 1,4-galactosyltransferase, polypeptide 5	0.8380	1.0131
B4galt6	UDP-Gal:betaGlcNAc beta 1,4-galactosyltransferase, polypeptide 6	0.0645	-1.2196
B4galt7	xylosylprotein beta1,4-galactosyltransferase, polypeptide 7 (galactosyltransferase I)	0.4116	-1.0764
Gck	glucokinase	0.0548	1.1856
Hk1	hexokinase 1	0.8593	1.0129
Hk2	hexokinase 2	0.4688	1.0771
Hk3	hexokinase 3	0.0236	-1.2237
Adpgk	ADP-dependent glucokinase	0.4033	-1.0787
Gpi1	glucose phosphate isomerase 1	0.7826	-1.0173
Gfpt1	glutamine fructose-6-phosphate transaminase 1	0.2410	-1.0941
Gfpt2	glutamine fructose-6-phosphate transaminase 2	0.0289	1.2116
Gnpda1	glucosamine-6-phosphate deaminase 1	0.6667	-1.0364
Gnpda2	glucosamine-6-phosphate deaminase 2	0.9474	1.0054

Table 1 continued on next page

Table 1 continued

Gene symbol	Gene description	p Value	Fold change
Gnpnat1	glucosamine-phosphate N-acetyltransferase 1	0.3646	-1.0839
Nat9	N-acetyltransferase 9 (GCN5-related, putative)	0.2253	1.0995
Pgm1	phosphoglucomutase 1	0.7697	-1.0243
Pgm2	phosphoglucomutase 2	0.7135	-1.0360
Pgm2l1	phosphoglucomutase 2-like 1	0.8036	-1.0167
Pgm3	phosphoglucomutase 3	0.6032	-1.0529
Pgm5	phosphoglucomutase 5	0.2374	1.1326
Uap1	UDP-N-acetylglucosamine pyrophosphorylase 1	0.6555	1.0402
Uap1l1	UDP-N-acteylglucosamine pyrophosphorylase 1-like 1	0.2637	-1.1092
Nagk	N-acetylglucosamine kinase	0.2907	-1.1126
Gale	galactose-4-epimerase, UDP	0.5196	1.0579
Gne	glucosamine (UDP-N-acetyl)-2-epimerase/N-acetylmannosamine kinase	0.2860	-1.0808

Gene symbol, gene description, p value and fold change of *Mgat2* deficient CD4⁺ T cells relative to control are shown. The microarray confirms loss of *Mgat2* expression, highlighted in bold.

DOI: 10.7554/eLife.14814.013

difference (**Figure 4D**). Thus, increased B3GNT enzyme activity is not responsible for the homeostatic up-regulation of poly-LacNAc induced by branching deficiency.

Homeostatic poly-LacNAc is not induced by alterations in UDP-GlcNAc levels

Next we investigated whether increased cellular UDP-GlcNAc, the donor substrate for B3GNT enzymes, is triggered by severe branching deficiency. Measurement of total cellular UDP-GlcNAc levels by mass spectrometry and/or a colorimetric assay in cell lysates of purified *Mgat2*^{+/+} versus *Mgat2*^{-/-} T cells as well as Jurkat T cells treated with or without SW and kifunensine revealed no increase from branching deficiency (**Figure 4E–G**). Supplementing cells with GlcNAc raises cellular UDP-GlcNAc and branching (**Lau et al., 2007; Mkhikian et al., 2011; Grigorian et al., 2007; Grigorian et al., 2011**). In contrast, treatment of Jurkat T cells with GlcNAc did not increase LEA staining despite a 3–4 fold increase in cellular UDP-GlcNAc concentrations; although it further enhanced SW induced poly-LacNAc extension (**Figure 4F,G**, and **Figure 4—figure supplement 1E**). Over-expression of the three UDP-GlcNAc Golgi transporters (SLC35A3, SLC35B4, and SLC35D2) via transfection into Jurkat T cells also did not increase LEA staining (**Figure 5F**). Thus, much like TCR signaling, increased cellular UDP-GlcNAc levels are neither necessary nor sufficient to induce homeostatic up-regulation of poly-LacNAc. Not surprisingly, poly-LacNAc induction was blocked by 4-Fluoro-GlcNAc, a drug known to inhibit poly-LacNAc production by reducing UDP-GlcNAc biosynthesis (**Barthel et al., 2011**) (**Figure 4—figure supplement 1F–G**).

UDP-GlcNAc redistribution from *Cis*/*Medial* to *Trans* Golgi triggers homeostatic poly-LacNAc

Glycosylation enzymes are organized in order of action from *cis* to *trans* along the secretory pathway. The branching enzymes (i.e. MGAT1, 2, 4 and 5) are localized to the *medial* Golgi, while the galactosyl transferase and B3GNT enzymes reside in the *trans* Golgi. The CMP-sialic acid transporter has a relatively restricted localization within the Golgi (**Zhao et al., 2006**), suggesting that sugar-nucleotide donors may be preferentially supplied to specific Golgi compartments. We hypothesized that UDP-GlcNAc supply and associated transporters may be restricted to the *cis/medial* Golgi compartment, thus preferentially driving branching over extension. Consistent with this hypothesis, raising total cellular UDP-GlcNAc increases branching by the *medial* Golgi enzymes (**Lau et al., 2007; Mkhikian et al., 2011; Grigorian et al., 2007; Grigorian et al., 2011**), but does not induce significant up-regulation of poly-LacNAc extension by *trans* Golgi B3GNT enzymes (**Figure 4F,G**, and **Figure 4—figure supplement 1E**). This suggests that cytosolic UDP-GlcNAc lacks direct access to the

Table 2. List of the top 50 differentially expressed genes.

Gene symbol	Gene description	p Value	Fold change
Rpl36al	ribosomal protein L36A-like	4.44E-16	-15.6258
Mgat2	mannoside acetylglucosaminyltransferase 2	9.43E-14	-27.8780
Fn1	fibronectin 1	5.83E-12	-7.5845
Cpm	carboxypeptidase M	3.54E-10	3.1233
Zbtb16	zinc finger and BTB domain containing 16	5.45E-10	-3.3239
Mmp9	matrix metalloproteinase 9	1.58E-09	-3.9658
Serpinb10-ps	serine (or cysteine) peptidase inhibitor, clade B (ovalbumin), member 10, pseudogene	4.39E-09	-5.0634
Zfp69	zinc finger protein 69	4.63E-09	-2.1283
Cd93	CD93 antigen	1.04E-08	-2.3236
Atp8a2	ATPase, aminophospholipid transporter-like, class I, type 8A, member 2	2.64E-08	-2.2711
Gpr141	G protein-coupled receptor 141	3.83E-08	-3.4035
Penk	preproenkephalin	5.28E-08	3.8411
Clec7a	C-type lectin domain family 7, member a	8.21E-08	-2.4336
Lyz1	lysozyme 1	1.06E-07	-3.4287
Mpeg1	macrophage expressed gene 1	1.18E-07	-4.3408
Klra2	killer cell lectin-like receptor, subfamily A, member 2	1.33E-07	-4.4037
Kit	kit oncogene	2.44E-07	-2.3150
Plbd1	phospholipase B domain containing 1	2.47E-07	-2.9529
Lyz2	lysozyme 2	2.83E-07	-3.6156
Pld4	phospholipase D family, member 4	3.00E-07	-4.1375
Ace	angiotensin I converting enzyme (peptidyl-dipeptidase A) 1	3.36E-07	-3.3758
Sirpa	signal-regulatory protein alpha	3.40E-07	-3.9975
Clec12a	C-type lectin domain family 12, member a	3.54E-07	-4.4547
Tlr13	toll-like receptor 13	4.15E-07	-6.5477
Tnfrsf21	tumor necrosis factor receptor superfamily, member 21	4.86E-07	-3.4333
Tgfb1	transforming growth factor, beta induced	5.57E-07	-3.6315
Adrbk2	adrenergic receptor kinase, beta 2	5.98E-07	-2.0416
Il12rb2	interleukin 12 receptor, beta 2	7.32E-07	-2.6927
Csf1r	colony stimulating factor 1 receptor	7.57E-07	-5.9870
Xcl1	chemokine (C motif) ligand 1	9.55E-07	-2.0969
Mlh1	mutL homolog 1 (E. coli)	9.66E-07	-2.0854
Sulf2	sulfatase 2	1.01E-06	-2.9791
Igfbp6	immunoglobulin superfamily, member 6	1.04E-06	-3.0615
Gpr56	G protein-coupled receptor 56	1.10E-06	-2.2352
Fcna	ficolin A	1.23E-06	-4.7706
Clec4a1	C-type lectin domain family 4, member a1	1.29E-06	-5.5202
Gm11428	predicted gene 11428	1.33E-06	-2.5636
Kcnj16	potassium inwardly-rectifying channel, subfamily J, member 16	1.35E-06	-2.5828
Coro2a	coronin, actin binding protein 2A	1.80E-06	1.5820
Clec4a3	C-type lectin domain family 4, member a3	1.88E-06	-4.7329
Muc13	mucin 13, epithelial transmembrane	1.91E-06	-2.0524
Abcd2	ATP-binding cassette, sub-family D (ALD), member 2	2.49E-06	-2.2046
Cd68	CD68 antigen	2.56E-06	-2.6229
Cd34	CD34 antigen	2.65E-06	-1.9429

Table 2 continued on next page

Table 2 continued

Gene symbol	Gene description	p Value	Fold change
Cxcr6	Sigmachemokine (C-X-C motif) receptor 6	2.68E-06	-3.3244
Mpo	myeloperoxidase	2.80E-06	-15.0742
Car1	carbonic anhydrase 1	2.95E-06	-10.5252
Pira11	paired-Ig-like receptor A11	3.03E-06	-3.3245
Emr1	EGF-like module containing, mucin-like, hormone receptor-like sequence 1	3.18E-06	-6.1010
Pira1	paired-Ig-like receptor A1	3.23E-06	-3.6538

Gene symbol, gene description, *p* value and fold change of *Mgat2* deficient CD4⁺ T cells relative to control are shown. Data are ordered by *p* value.

DOI: 10.7554/eLife.14814.014

trans Golgi compartment. To further evaluate this hypothesis, we examined the subcellular localization of the three UDP-GlcNAc Golgi transporters (SLC35A3, SLC35B4, and SLC35D2) and B3GNT2. Jurkat T cells were transfected with DDK or HA tagged versions of these proteins and examined for intra-Golgi localization using confocal microscopy-based line scan analysis. Intra-Golgi localization was determined by co-staining transfected cells with the *cis* and *trans* markers GM130 and TGN46, respectively, and determining the peak intensity of fluorescence along a line scan relative to these markers (Dejgaard et al., 2007). All three UDP-GlcNAc transporters localized to the *cis* and *medial* Golgi compartments while B3GNT2 localized to a later Golgi compartment (Figure 5A–E). In addition, overexpression of the UDP-GlcNAc transporters did not drive poly-LacNAc production (Figure 5F). These results suggest that the *trans* Golgi is comparatively deficient in UDP-GlcNAc, thereby limiting B3GNT activity and poly-LacNAc extension under steady state conditions.

As B3GNT requires UDP-GlcNAc to generate poly-LacNAc, we reasoned that these two factors must co-localize to drive homeostatic up-regulation of poly-LacNAc following disruption of branching activity. Co-localization may arise from movement of UDP-GlcNAc transporters to the *trans* Golgi and/or movement of B3GNT to the *medial* Golgi. However, SW treatment did not alter the Golgi localization of the three UDP-GlcNAc transporters or B3GNT2, arguing against this possibility (Figure 5E and Figure 5—figure supplement 1A–D). Alternatively, UDP-GlcNAc may directly shift from the *medial* to *trans* Golgi via the inter-cisternal transport system. Significant loss of activity of *medial* Golgi branching enzymes should acutely raise UDP-GlcNAc levels within the *medial* Golgi, with excess UDP-GlcNAc subsequently moving forward to the *trans* Golgi via inter-cisternal diffusion. Measuring UDP-GlcNAc by LC-MS/MS in a whole cell vesicular fraction isolated from post nuclear supernatant revealed significant levels of UDP-GlcNAc (Figure 6—figure supplement 1A–B). To ensure that UDP-GlcNAc was indeed within the vesicles as opposed to merely associated with the outer membrane, the post nuclear supernatant (PNS) was treated with either 0.1% Triton-X or 50 mM uridine monophosphate (UMP) for 15 min prior to isolation of the vesicular fraction by ultracentrifugation. Both treatments significantly reduced the amount of UDP-GlcNAc in the vesicular fraction, confirming UDP-GlcNAc was located in vesicles containing UDP-GlcNAc/UMP anti-porters (Figure 6—figure supplement 1B–D).

To evaluate the effects of reduced branching activity in the *medial* Golgi, we compared Jurkat T cells treated with and without kifunensine. Consistent with our hypothesis, UDP-GlcNAc levels were elevated in the vesicular but not the cytosolic fractions of kifunensine treated Jurkat T cells (Figure 6A). To examine the Golgi directly, we used antibodies to the *trans* marker TGN46 to immuno-isolate a Golgi enriched fraction from Jurkat T cell PNS. As expected from the physical connections between Golgi cisterna, western blotting for *cis*, *medial*, and *trans* Golgi markers confirmed that all three cisternal compartments were recovered with anti-TGN46 (Figure 6B). UDP-GlcNAc was elevated in the Golgi of kifunensine treated Jurkat T cells despite no difference in total cellular or cytosolic UDP-GlcNAc levels (Figures 4G, 6A, C). Finally, we isolated a fraction enriched for *trans*-Golgi network (TGN) vesicles from Jurkat T cells by pretreating with Brefeldin A prior to pull down with anti-TGN46. Brefeldin A separates the *trans*-Golgi network from the rest of the Golgi by fusing the latter with the endoplasmic reticulum (Martínez-Alonso et al., 2013). TGN46 immuno-isolated vesicles from Brefeldin A treated Jurkat T cells were partially depleted for *cis* and *medial* Golgi markers relative to *trans* Golgi markers including B3GNT2, confirming relative enrichment of the

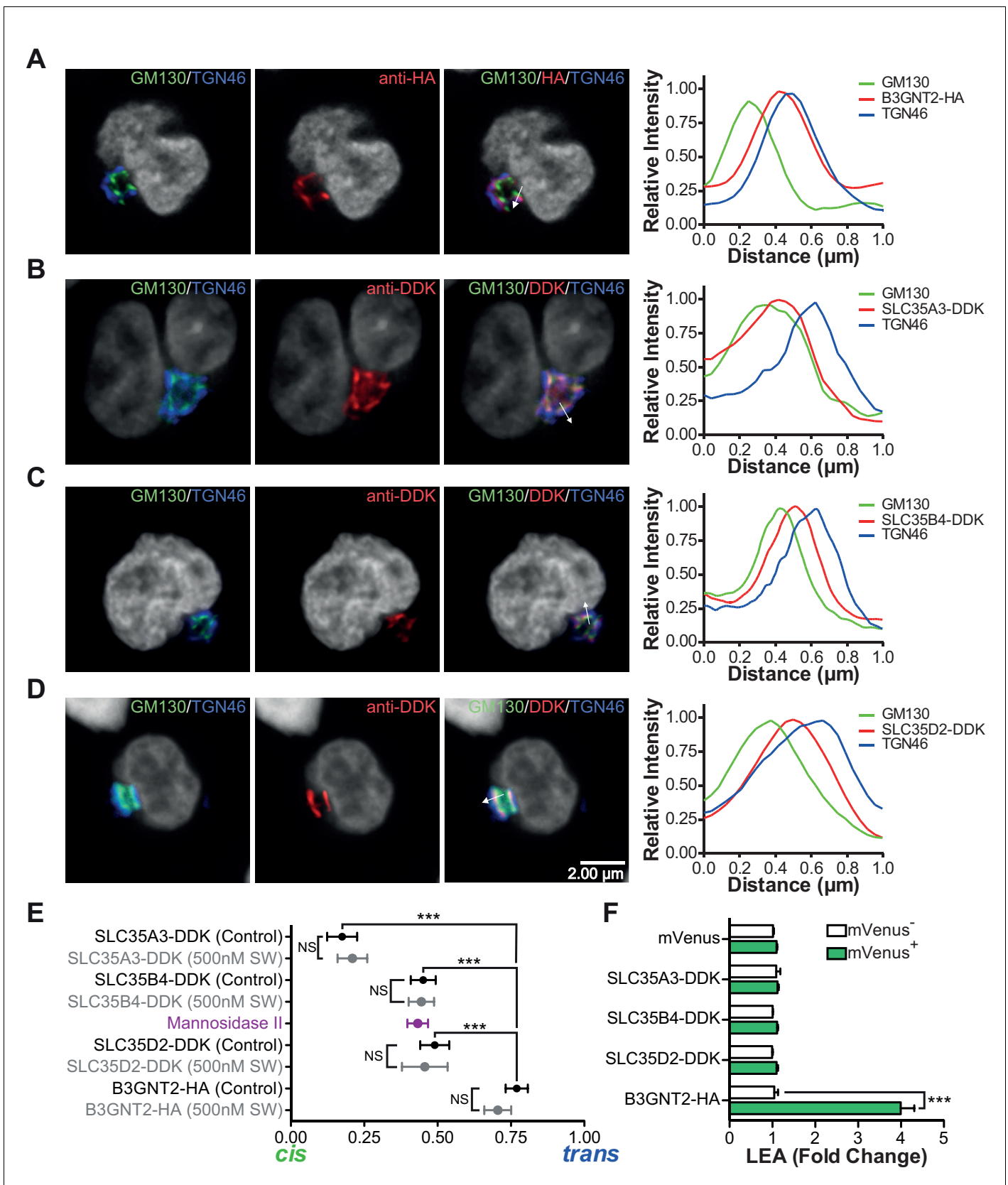


Figure 5. The UDP-GlcNAc transporters are localized to an earlier Golgi compartment than B3GNT2. (A–D) Jurkat T cells were transfected with plasmids containing B3GNT2-HA (A), SLC35A3-DDK (B), SLC35B4-DDK (C), or SLC35D2-DDK (D), cultured for 24 hr and then stained for GM130
 Figure 5 continued on next page

Figure 5 continued

(green), TGN46 (blue) and either anti-HA (A) or anti-DDK (B–D) in red. Shown are representative confocal slices from transfected cells. The white arrows demonstrate areas deemed suitable for line scan analysis and the histograms (far right) demonstrate signal intensities along the line scans. DAPI staining is shown in grey scale. (E) Average localizations of the indicated Golgi proteins in Jurkat T cells treated with and without swainsonine (see **Figure 5—figure supplement 1**) relative to GM130 (*cis*) and TGN46 (*trans*) markers. Error bars show standard deviation. (F) Jurkat cells were transfected with mVenus alone or in combination with the four constructs of interest. After 48 hr, cells were analyzed for LEA binding by flow cytometry gating on mVenus⁻ and mVenus⁺ cells as indicated. NS, not significant; **p*<0.05; ***p*<0.01; ****p*<0.001 (unpaired two-tailed t-test with Welch's (E and F) and Bonferroni correction (E)). Data show images and histograms from representative cells (A–D), or pooled analysis from 30–40 cells per condition (E). Error bars indicate mean ± S.D. (E) or mean ± s.e.m (F).

DOI: 10.7554/eLife.14814.015

The following figure supplement is available for figure 5:

Figure supplement 1. Branching deficiency does not cause relocalization of the UDP-GlcNAc transporters or B3GNT2.

DOI: 10.7554/eLife.14814.016

trans/TGN compartment (**Figure 6D and E**). Vesicles from kifunensine treated Jurkat T cells demonstrated increased UDP-GlcNAc relative to control (**Figure 6F**), indicating that UDP-GlcNAc levels rise in the *trans* Golgi when *medial* Golgi branching activity is significantly diminished.

Although the mechanism for cargo transport between Golgi cisterna is incompletely understood, the prevailing model is cisternal maturation, where entire cisterna move forward with their cargo, while Golgi enzymes/transporters are pulled back to earlier cisterna by vesicular transport (**Glick and Luini, 2011**). However, this model has recently been expanded by data suggesting that small cargo transits the Golgi by diffusion via inter-cisternal tubules that vertically connect the *cis*, *medial*, and *trans* compartments (**Martínez-Alonso et al., 2013; Beznoussenko et al., 2014; Trucco et al., 2004**). Indeed, at least in CHO cells, there is evidence for functional continuity throughout sub-compartments of the Golgi (**Kim et al., 2001**). Golgi stacks, consisting of the *cis*, *medial*, and *trans* compartments, are also connected longitudinally to other Golgi stacks by tubules. Nocodazole, which interrupts longitudinal but not vertical Golgi tubules, had no effect on poly-LacNAc induction by SW in Jurkat T cells (**Figure 6G**). In contrast, pyrrophenone disrupts both longitudinal and inter-cisternal vertical tubules via inhibition of cytosolic phospholipase A₂-α (**San Pietro et al., 2009**). Pyrrophenone significantly blocked SW induced up-regulation of poly-LacNAc in Jurkat T cells in a dose dependent manner, as indicated by comparing its effects on LEA and ConA staining; the latter controlling for any changes in Golgi transport (**Figure 6H and Figure 6—figure supplement 1E**). In contrast, pyrrophenone had no effect on ConA, LEA, or L-PHA levels in control Jurkat T cells lacking SW (**Figure 6—supplement figure 1F–H**). We conclude that when branching enzymes under-utilize UDP-GlcNAc in the *medial* Golgi, UDP-GlcNAc accumulates and then shifts by diffusion to the *trans* Golgi via inter-cisternal tubules, thereby increasing substrate supply to B3GNT and triggering poly-LacNAc extension (**Figure 7**). However, our data do not exclude additional transfer of UDP-GlcNAc via vesicles or by cisternal maturation.

Discussion

Our data demonstrates that structurally disparate glycans are functionally equivalent based on LacNAc content and suggests a novel self-correcting mechanism in the Golgi that sustains cellular homeostasis by ensuring LacNAc content is maintained at a minimal level within N-glycans. The complexity of glycan structures provides tremendous challenges for discerning the functional role of glycans in biology. Although N-glycan structures are highly diverse, redundancy of structural motifs within individual glycans has previously received little consideration as a means to collapse complexity and decipher glycan information. Deficiency of glycosylation pathway genes often give rise to new and unusual structures, triggering some to suggest that these may represent compensatory structures (**Stone et al., 2009; Takamatsu et al., 2010; Ismail et al., 2011; Dam and Brewer, 2010; Dennis and Brewer, 2013**). However, proof of functional equivalency has largely been lacking. The similar degree of hyperactivity between *Mgat5* and *Mgat2* deficient T cells indicates that poly-LacNAc extended hybrid structures are functionally equivalent to complex tri-antennary structures. Importantly, blockade of mannosidase II and *Mgat2* deficiency produced a similar phenotype, which was blocked/reversed by both mannosidase I inhibition and *Mgat1* deficiency, despite each targeting distinct biochemical steps and resulting in distinct structures. Thus, our data demonstrate that

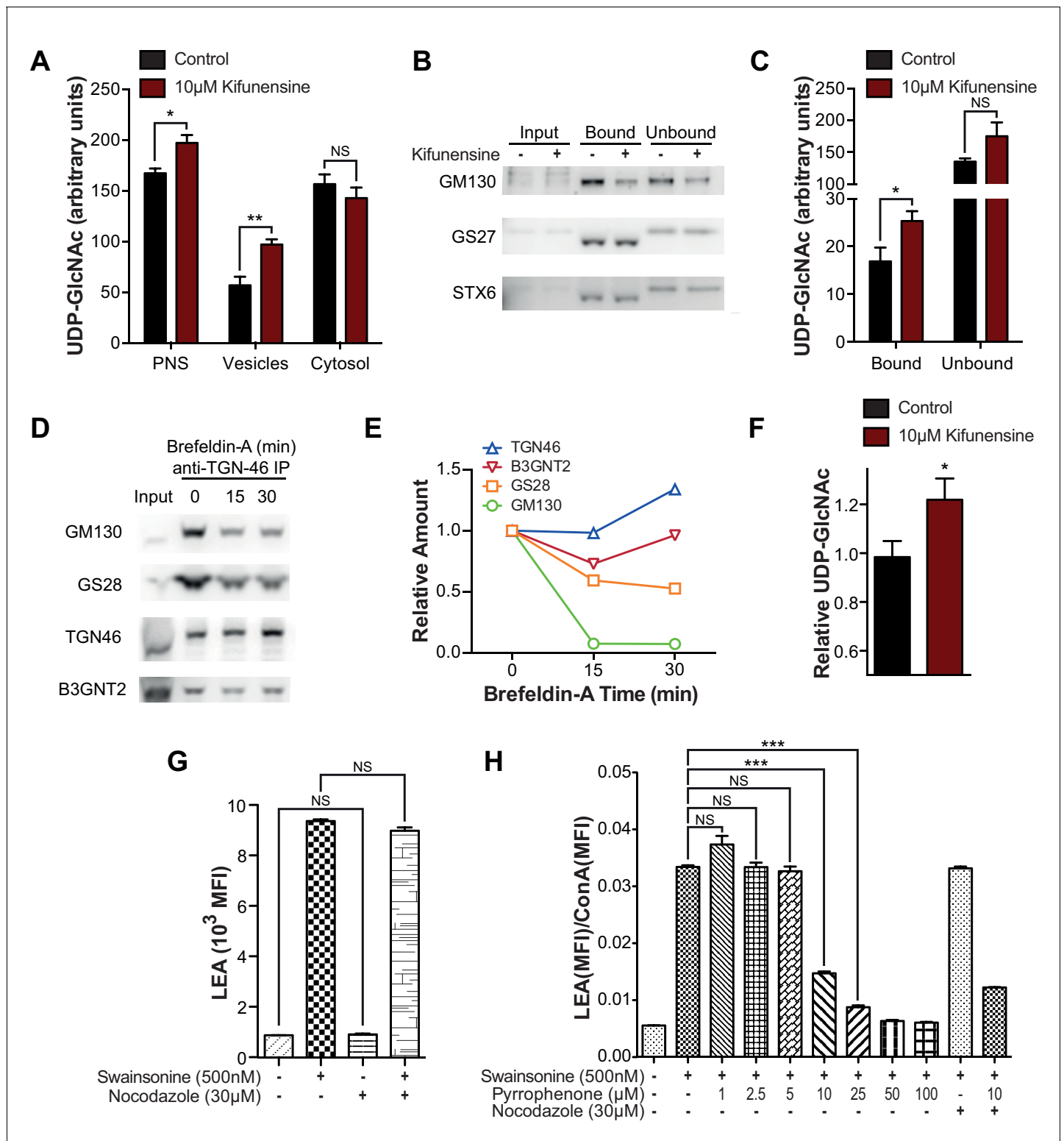


Figure 6. Intra-Golgi UDP-GlcNAc shifts to later Golgi compartments when use in the medial Golgi is inhibited. (A) LC-MS/MS quantitation of UDP-GlcNAc in post-nuclear supernatants (PNS), vesicular, and cytosolic fractions of kifunensine treated and untreated Jurkat T cells. (B) PNS (input) from kifunensine treated and untreated Jurkat T cells was used for Golgi enrichment via anti-TGN46 immuno-isolation followed by blotting for the Golgi compartment markers GM130 (*cis*), GS27 (*medial/trans*), and Syntaxin6 (*trans*). (C) LC-MS/MS quantitation of UDP-GlcNAc in anti-TGN46 bound and unbound fractions from kifunensine treated and untreated Jurkat T cell PNS. (D) PNS of Jurkat T cells treated for 0, 15, and 30 min with the Golgi disruptor Brefeldin A were used for anti-TGN46 immuno-isolation followed by blotting for B3GNT2 and the GM130 (*cis*), GS28 (*cis/medial*), and TGN46

Figure 6 continued on next page

Figure 6 continued

(*trans*) Golgi markers. (E) Quantitation of D, (F) LC-MS/MS quantitation of UDP-GlcNAc in anti-TGN46 immuno-isolates from Jurkat cells treated with Brefeldin A for 15 min. (G) LEA flow cytometric analysis of Jurkat T cells pre-treated with nocodazole where indicated for 45 min, followed by swainsonine where indicated for 5 hr. (H) Jurkat T cells that were treated with nocodazole +/- pyrrophenone as indicated for 45 min were treated with or without swainsonine for 5 hr and then analyzed for LEA and ConA binding by flow cytometry. Shown is the ratio of LEA MFI to ConA MFI for each condition. NS, not significant; * $p < 0.05$; ** $p < 0.01$; *** $p < 0.001$; (unpaired one-tailed (A, C, F and G) or two-tailed (H) t-test with Welch's correction and Bonferroni correction (H)). Data show one experiment representative of at least three independent experiments except F which shows combined data from two independent experiments. Error bars indicate mean \pm s.e.m.

DOI: 10.7554/eLife.14814.017

The following figure supplement is available for figure 6:

Figure supplement 1. Intra-Golgi UDP-GlcNAc shifts to later Golgi compartments when use in the *medial* Golgi is inhibited.

DOI: 10.7554/eLife.14814.018

structurally diverse glycans are biologically equivalent if they share a similar amount of LacNAc. The overall glycan structure sets the total LacNAc content, thereby largely determining avidity of binding for galectins. It should be noted however, that although these differing glycoforms are clearly

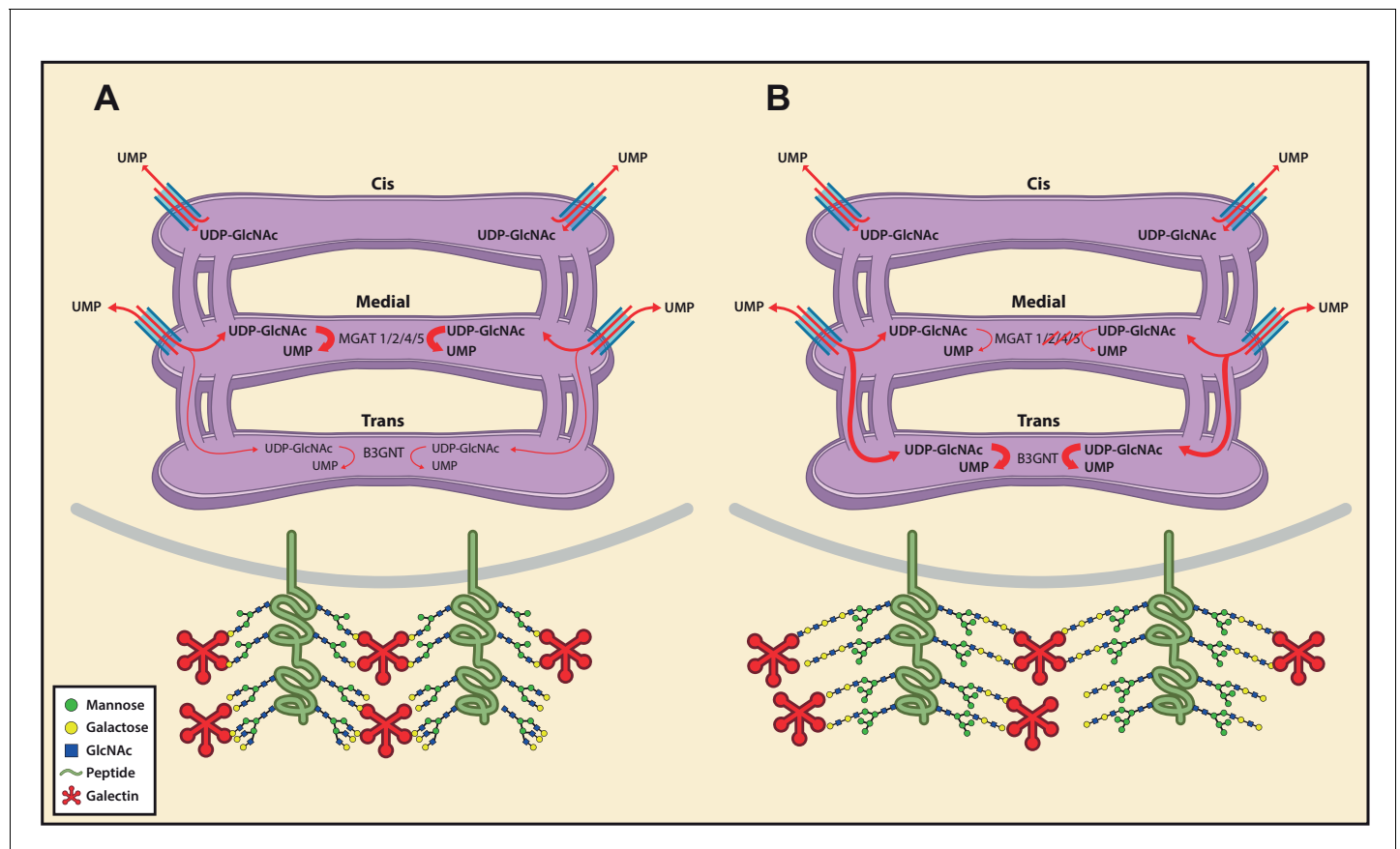


Figure 7. Model of an inherent Golgi self-correcting mechanism to maintain LacNAc homeostasis. The majority of UDP-GlcNAc entering the Golgi is supplied to its early compartments by the UDP-GlcNAc/UMP antiporters, which are preferentially localized to the *cis/medial* Golgi. Under branching proficient conditions (A), UDP-GlcNAc is used by the branching enzymes MGAT1, 2, 4, and 5, with little unused UDP-GlcNAc supplying the poly-LacNAc synthesizing B3GNT enzymes. The resulting array of N-glycans produced thus contains more LacNAc branches than linear LacNAc polymers (A). When the branching pathway is disrupted (B), or presumably the Golgi is otherwise stressed, leading to reduced UDP-GlcNAc usage in the *medial* Golgi, UDP-GlcNAc is driven forward (at least partially through intercisternal tubules) and promotes production of bioequivalent poly-LacNAc containing glycans by the *trans* Golgi-resident B3GNT family of enzymes. Under this scenario, loss of LacNAc branches is balanced by increased production of linear LacNAc polymers, a self-correcting ability that serves to maintain cell surface LacNAc density and thus the galectin-glycoprotein lattice (A). In the context of T cells, this homeostatic mechanism acts to curtail catastrophic T cell hyperactivity and promotes self-tolerance.

DOI: 10.7554/eLife.14814.019

overlapping, they might not be strictly identical due to distinct geometries of LacNAc presentation or modification by fucose or sialic acid.

Our data support a model of N-glycosylation that emphasizes the significance of functional units within an N-glycan, such as LacNAc groups, rather than uniqueness of the overall glycan structure in determining biological function. The National Academy of Sciences position paper on Glycoscience has proposed a major focus on glycan structural determination (**National Academy of Sciences, 2012**). Our data suggests that glycan diversity may be collapsed into a much smaller group of bio-equivalent structures based on the number of structural subunits within the overall glycan that bind to a given animal lectin. Indeed, it may be possible that through further studies exploring bioequivalence among glycans, a glycan code can be deciphered based on interaction with animal lectins. Such an approach may greatly alleviate the complexity in determining structure-function relationships and relevance to human health.

Essential biological systems employ homeostatic mechanisms to maintain cellular integrity. N-glycosylation is an essential biosynthetic pathway necessary for cellular homeostasis and mammalian development (**Dennis et al., 2009**), yet lacks a known self-correcting mechanism. Our data suggest that homeostatic control of LacNAc content does not result from changes in enzyme levels/activity or metabolic production of UDP-GlcNAc substrate; but rather appears to arise from the structure of the Golgi. A defining feature of the Golgi is its polarized compartmentalization, with a *cis* to *trans* organization. Glycosylation enzymes are arranged along the Golgi roughly in the order in which they act. Why the Golgi has evolved this organization remains an open question. Our data indicate that the UDP-GlcNAc transporters preferentially supply UDP-GlcNAc to the *cis/medial* over *trans* Golgi, thus prioritizing branching over extension. Despite the presence of continuities between Golgi cisterna and previous work arguing that the Golgi is functionally interconnected (**Kim et al., 2001**), our data suggest that the segmented organization of enzymes and transporters allows for local depletion of substrate prior to diffusion to other compartments. In this manner, the evolutionary placement of the B3GNT poly-LacNAc extension enzymes in the *trans* Golgi provides a backup mechanism that captures unused UDP-GlcNAc from the *medial* Golgi shunted via inter-cisternal tubules. This backup system may also explain the lack of evolutionary pressure to produce genetic redundancy in the Golgi branching enzymes in mammals and the dramatically more severe phenotype seen with *Mgat1* deficiency, which blocks all production of N-glycan LacNAc, compared to other *Mgat* genes (**Ioffe and Stanley, 1994; Metzler et al., 1994**).

The Golgi is charged with maintaining the integrity of the glycome/lattice or risking disease. Thus, fidelity of glycan biosynthesis must be maintained under a variety of cellular states and be active virtually at all times. High protein transit rates present a significant challenge to the Golgi and have the potential to reduce the *medial* Golgi branching efficiency by decreasing the time available for branching reactions. Under this scenario, having a back-up system that provides poly-LacNAc extension in the *trans* Golgi by capturing unused UDP-GlcNAc from the *medial* Golgi would be critical for the maintenance of the lattice at a minimal essential level. Even in an unstressed system, a second step in the assembly line would act to counteract the moment to moment variability and stochastic uncertainty of glycan synthesis. Severe branching deficiency (induced by SW treatment or *Mgat2* deletion) uncovers this continual process. Such a mechanism is akin to DNA repair, which is occurring all of the time but made more apparent in the context of physiological or external stress.

A clear understanding of the network of interacting factors that coalesce to determine the state of the galectin-glycoprotein lattice is required for the successful exploitation of its therapeutic potential. Interventions must be able to overcome or at least take into account the homeostatic cellular response to the initial disturbance. For example, the effectiveness of SW as an anti-cancer therapeutic is likely limited by compensatory poly-LacNAc production (**Goss et al., 1994; 1997**). Thus, therapeutic strategies aimed at disrupting the lattice should block branching and extension simultaneously, or target a more proximal regulator such as UDP-GlcNAc metabolism or transport. In light of these considerations, the lattice approach to cancer treatment may merit re-visitation. Conversely, a deeper knowledge of the central regulatory machinery that determines total LacNAc content will also be required for therapeutic approaches that seek to strengthen the lattice.

The presence of functional groups (LacNAc) as subcomponents of glycans, combined with our current understanding of Golgi transport, may also explain the curious use of three different nucleotides to charge the array of sugars used as substrate donors for glycosylation. These sugar-nucleotides are transported into the Golgi via an anti-port mechanism where cytosolic sugar-nucleotides are

exchanged for Golgi nucleotides generated by the action of glycosyltransferase enzymes. Increased availability and use of UDP-GlcNAc in the *trans* Golgi would increase uridine-monophosphate (UMP) levels, thereby driving anti-port of UDP-Galactose into the *trans* Golgi to promote further extension with poly-LacNAc rather than capping by sialic acid. Were sialic acid also charged with UDP rather than cytidine-monophosphate (CMP), UDP-GlcNAc usage in the *trans* Golgi would drive import of UDP-Sialic acid and capping equally with UDP-Galactose and extension.

Materials and methods

Galectin-3 binding

Recombinant mouse galectin-3 (R&D Systems, Minneapolis, MN) was labeled using an Alexa Fluor 488 protein labeling kit (ThermoFisher Scientific, Waltham, MA). Cells were stained for flow cytometry using 3 μ g labeled galectin-3 per test. Staining was carried out for 30 min at room temperature followed by one wash and fixation with paraformaldehyde. For the lactose control samples, 50 mM lactose was included in all steps.

PNGase F treatment of live cells

Purified mouse T cells were washed twice in HBSS and resuspended in 100 μ l of G7 reaction buffer. 2500 units of glycerol free PNGase F (New England Biolabs, Ipswich, MA) was added to the cells and the reaction was allowed to proceed for up to four hours at 37 degrees Celsius. Cells were then washed with HBSS and immediately stained for flow cytometry.

MALDI-TOF mass spectrometry

Control and SW treated Jurkat T cells were homogenized by sonication in 25 mM Tris, 150 mM NaCl, 5 mM EDTA, and 1% CHAPS, pH 7.4, dialyzed, reduced, and carboxymethylated, digested with trypsin to generate glycopeptides and treated with PNGase F (Roche, Basel, Switzerland) to release N-glycans. N-glycans were digested by endo- β -galactosidase (AMS Biotechnology) or Sialidase A (Prozyme, Hayward, CA) prior to permethylation and mass spectrometry analysis.

Cell lines

Human Jurkat cell line E6-1 and its derivative cell lines with deficiency in TCR β (J.RT3-T3.5), and Lck (J.CaM1.6) were purchased from ATCC. Two separate lots of E6-1 Jurkat cells were purchased throughout the study and found to be equivalent in LEA increase in response to SW treatment. Cells were cultured, expanded and frozen down to create low passage stocks. These were subsequently thawed and used for experiments, limiting usage to a maximum of ten passages. They were grown in RPMI 1640 medium with 10% fetal bovine serum, 2 mM L-glutamine, 100 U/ml penicillin/streptomycin and 2 μ M 2-mercaptoethanol. CFPAC-1, CHO, Lec1, Raji, RPMI 8226, RS4; 11 and Kasumi-1 cell lines were also purchased from the ATCC. BJ, HT-29 and HEK-293 cells were a kind gift from Bogi Andersen. MCF-7 and HeLa cells were a kind gift from Marian Waterman. Mouse postnatal day 1 neural stem cells were a kind gift from Thomas Lane. HUVEC cells were a kind gift from Christopher Hughes, and K562 cells were a kind gift from David Fruman. No routine mycoplasma testing or identity authentication was performed.

Reagents, mice and flow cytometry

Isolated human CD3⁺ T cells purified by negative selection (RosetteSep, StemCell Technologies, Vancouver, Canada) were stimulated with plate-bound anti-CD3 (OKT3, eBioscience, San Diego, CA). Procedures with human subjects were approved by the Institutional Review Board of the University of California, Irvine. *Mgat2^{fl/fl}* (006892), *Mgat1^{fl/fl}* (006891) and *Lck-Cre* (003802) mice were obtained from Jackson Laboratory. *B3gnt2^{+/-}* (11605) embryos were from the MMRRC and were rederived by the UC Irvine Transgenic Mouse Facility. Inter-breeding generated all other mice. Mice were selected randomly for experiments and approved by the Institutional Animal Care and Use Committee of the University of California, Irvine. Human cells were stained with anti-CD4, anti-CD69 (eBioscience) and/or L-PHA-FITC (*Phaseolus Vulgaris* Leukoagglutinin, Vector Labs, Burlingame, CA). Mouse cells were stained with anti-CD4 (RM 4–5), anti-CD8 (53–6.7), and anti-CD69 (H1.2F3) (eBioscience). Proliferation was assessed by 5, 6-carboxyfluorescein diacetate

succinimidyl ester (CFSE; ThermoFisher Scientific) at 1 μ M in PBS (20 min., 4°C) and stimulated with plate-bound anti-CD3e. Cells were cultured in RPMI-1640 media supplemented with 10% fetal bovine serum, 2 μ M L-glutamine, 100 U/ml penicillin/streptomycin and 2 μ M 2-mercaptoethanol. Where indicated, 40 mM GlcNAc (Ultimate Glucosamine, Wellesley Therapeutics Inc., Toronto, Canada) and 10 mM uridine (Sigma-Aldrich, St Louis, MO) were added to cells in culture at time 0. For flow cytometric analysis of glycan expression, cells were stained with 2 μ g/ml L-PHA-FITC, ConA-FITC, LEA-FITC or biotinylated versions of these lectins followed by DyLight649 labeled streptavidin (Vector Labs). Staining was carried out as previously described (Lee et al., 2007; Grigorian et al., 2007). Flow cytometry experiments were performed with the BD FACSCalibur, LSR II, or Attune Acoustic Focusing Cytometer. Data analysis was performed using FlowJo software.

RNA isolation and microarray

CD4⁺ T cells isolated from *Mgat2^{fl/fl}* mice and L-PHA⁻CD4⁺ T cells isolated from *Mgat2^{fl/fl}::Lck-Cre⁺* mice were used for analysis. The RNeasy mini kit (Qiagen, Valencia, CA) was used for RNA extraction. Gene expression was assessed using the Affymetrix Mouse Gene 1.0 ST arrays in triplicate. Array data were quantified with Expression Console version 1.1 software (Affymetrix, Santa Clara, CA) using the PLIER Algorithm default values. Expression values were then filtered as present/absent at expression 100. The Cyber-T web server was used for data analysis and to compare samples.

Enzymatic assays

B3GNT enzyme activity was measured using a glycosyltransferase activity kit (R&D systems). Five million Jurkat cells grown with or without SW were washed three times with Tris buffered saline and lysed with 300 μ l of lysis buffer (10 mM Tris pH 7.5, 2 mM MnCl₂, 4 mM CaCl₂, 0.5% Triton-X, with protease inhibitors). The lysate was cleared of insoluble material by centrifugation and dialyzed overnight in an identical solution to remove cellular phosphate. Enzyme activity was measured following the instructions of the kit. Briefly, 25 μ l of lysate was mixed with 25 μ l of reaction mixture to give a final concentration of 6 mM N-acetyllactosamine, 5 mM UDP-GlcNAc, and 6 ng/ μ l coupling phosphatase. The reaction was allowed to proceed for two hours at 37°C, followed by visualization of released phosphate by a malachite green reagent as indicated in the kit. Absorbance at 620 nm was determined using a plate reader and converted using a phosphate standard run in parallel. Background was determined and subtracted by parallel reactions that lacked the specific acceptor N-acetyllactosamine but contained UDP-GlcNAc and coupling phosphatase.

Experimental autoimmune encephalomyelitis

EAE was induced by subcutaneous immunization of randomly selected female mice at days 0 with 100 μ g of bovine MOG35-55 (AnaSpec, Fremont, CA) emulsified in Complete Freund's Adjuvant containing 4 mg/ml heat-inactivated *Mycobacterium tuberculosis* (H37RA; Difco). On days 0 and 2, mice received 150 ng of pertussis toxin (List Biological Laboratories, Campbell, CA) by intraperitoneal injection. Mice were examined daily for clinical signs of EAE over the next 30 days with observer blinded to treatment conditions. Mice were scored daily as follows: 0, no disease; 1, loss of tail tone; 2, hindlimb weakness; 3, hindlimb paralysis; 4, forelimb weakness or paralysis and hindlimb paralysis; 5, moribund or dead. Kifunensine was given orally via the drinking water at 0.2 mg/ml for 8 days starting 3 days before immunization. All mice were housed with 12 hr light/dark cycles.

Spectrophotometric measurement of UDP-GlcNAc

UDP-GlcNAc was measured spectrophotometrically as previously described (Barthel et al., 2011). Briefly, Jurkat cells were grown in various conditions, washed thoroughly with PBS and pelleted at 50×10^6 cells per 1.5 ml tube. Cells were lysed by addition of 200 μ l of chloroform/water (1:1), vortexed for 2 min and centrifuged at $15,000 \times g$ for 20 min at 4°C. The aqueous phase was transferred to a fresh tube and 10 μ l of 1 N HCl was added to hydrolyze UDP-GlcNAc to GlcNAc. After heating for 20 min at 80°C, the sample was neutralized with 10 μ l 1 N KOH. Next, 50 μ l of 200 mM potassium tetraborate (Sigma-Aldrich) was added, and the sample was heated at 80°C for 25 min and then cooled on ice for 5 min. 150 μ l of Ehrlich's reagent (Sigma-Aldrich) (diluted 1:2 in acetic acid)

was added to the sample, mixed, and incubated for 20 min at 37°C. The sample was centrifuged at $15,000 \times g$ for 20 min, 200 μ l were added to a 96-well plate, and the absorbance was measured at 595 nm. Absorbance was converted to UDP-GlcNAc concentration by comparing to a GlcNAc standard curve run simultaneously.

UDP-GlcNAc measurement by LC-MS/MS

Jurkat and mouse T cells were treated as described in the text, then harvested, washed twice with ice-cold 1x PBS and counted. After normalizing for cell number, cells were pelleted in 1.5 ml Eppendorf tubes by centrifuging at 350 g for 7 min at 4°C. Metabolites were extracted from the pellets by the addition of 1 ml of ice-cold solution of 40% acetonitrile, 40% methanol, and 20% water. The tubes were vortexed for 1 hr at 4°C and spun down at 14000 rpm for 10 min at 4°C (Eppendorf, Hamburg, Germany). The supernatant was transferred to fresh tubes and evaporated to dryness in an Eppendorf Vacufuge at 30°C (Eppendorf). The dry samples were stored at -80°C until analysis at which point they were reconstituted in 100 μ l of LC-MS grade water and centrifuged again at 14000 rpm for 10 min at 4°C. The supernatants were carefully transferred to fresh tubes to be analyzed by mass spectrometry. The instrument used was a Waters Quattro Premier XE LC-MS/MS (Manchester, UK) equipped with ultra-performance liquid chromatography (UPLC) and a refrigerated autosampler. The separation was performed on BEH C18 reversed phase column (Waters, Manchester, UK) with a mobile phase A containing LC-MS grade water (JT Baker) modified with 0.2% Acetic Acid, 2% Acetonitrile and 5 mM Ammonium Acetate while mobile B containing LC-MS grade Acetonitrile (JT Baker) modified with 0.2% Acetic Acid and 5 mM ammonium Acetate. The gradient was performed with a 1 min ramp from 2% mobile B to 90%, which was then kept at 90% for 1 more minute and ramped back to 2% for column equilibration. The mass spectrometry measurement was performed in negative mode where the parent ion and fragment ion were measured simultaneously to be used for quantitation of the metabolites. A standard curve was generated using UDP-GlcNAc (Sigma-Aldrich), which was used for the quantitation of the metabolites produced by the cells.

Cellular subfractionation and Golgi immunoisolation

Jurkat cells were grown with or without kifunensine for four days, or until cultures reached a density between $1.5\text{--}2 \times 10^6$ cells/ml. Cells used for Golgi compartment disruption were treated with 1000x Brefeldin A (eBioscience 00-4506-51) for up to 30 min. Cells were washed with HEPES buffered saline (145 mM NaCl, 100 μ M HEPES, pH 7.4) and incubated in an ice-cold hypotonic solution (30 mM KCl, 3 mM MgOAc, 2 mM DTT, 20 mM HEPES, pH 7.5) for 5 min on ice. The volume of the hypotonic solution used was 2.5 times the volume of the cell pellet. The cell solution was then passed through a 26.5 gauge syringe five times before a 1/10 volume of ice-cold hypertonic solution (375 mM KCl, 22.5 mM MgOAc, 1 mM DTT, 220 mM HEPES, pH 7.5) was added. The solution was centrifuged twice in succession at 1000x g for 5 min each to pellet cells and nuclei. The post-nuclear supernatant (PNS) was carefully transferred to a new tube and processed further. Ultracentrifugation of the PNS at 100,000 g for 30 min yielded a vesicular fraction (the pellet) and a cytosolic fraction (the supernatant). For immunoisolation experiments, PNS was incubated with anti-TNG46 antibody (Sigma-Aldrich T7576-200UL) previously conjugated to Protein G Dynabeads (ThermoFisher Scientific) for 30 min at 4°C with tumbling. Supernatant was removed, and immunoisolated Golgi was washed with HEPES buffered saline before processing for mass spectrometry or immunoblot analysis.

Plasmids, transfection and microscopy

DNA encoding mVenus and human *B3GNT2* (HA tagged at the C terminus) were codon-optimized for human expression, synthesized, and cloned into the pmax Cloning vector (Lonza, Basel, Switzerland). Myc-DDK tagged human *SLC35A3* (RC215108), *SLC35B4* (RC203263), and *SLC35D2* (RC218472) cDNA clones were purchased from Origene (Rockville, MD) in pCMV6 expression vectors. Cells were transfected with each construct individually (for microscopy) or in combination with mVenus to label transfected cells (for flow cytometry). 10^6 cells were transfected with 4–8 μ g of DNA using an Amaxa Nucleofector IIb set to program G-10. Cells were immediately transferred to pre-equilibrated media in 6 well plates and placed in the tissue culture incubator. After 5 hr, media was changed and pharmacological treatments were started. For localization

studies, cells were transferred to poly-L-lysine coated chamber slides (Falcon) after 24–48 hr of treatment. Cells were incubated in the chamber slides for 15 min to allow attachment to the slides and then fixed for 1 hr with 4% paraformaldehyde in PBS. Standard immunocytochemical staining was performed. Permeabilization was achieved with 0.1% saponin (Sigma-Aldrich). Primary antibodies used were to GM130 (Clone 35, BD Biosciences, Franklin Lakes, NJ), TGN46 (AbD Serotec, Hercules, CA), Mannosidase II (a kind gift from Dr. Christine Suetterlin), HA (ab9110, Abcam, Cambridge, UK), and DDK (Clone 4C5, Origene). Slides were stained with the appropriate secondary antibodies conjugated to Alexa Fluor (AF) 488, 555 and 647 and mounted with Prolong Gold Antifade reagent with DAPI (ThermoFisher Scientific). GM130 and TGN46 were always visualized with AF 488 and 647 respectively, while the protein of interest was visualized with AF 555. Slides were imaged on a Zeiss LSM 780 confocal microscope using a Zeiss plan-apochromat 100x oil objective with numerical aperture of 1.4. Localization of the proteins of interest was determined relative to GM130 and TGN46 using a line-scan method essentially identical to a previously published report (*Dejgaard et al., 2007*). Briefly, 30–50 transfected cells were imaged per experimental condition. Files were coded to blind the analyzer to treatment and protein of interest. Images were imported into the Zeiss Zen software (blue edition) with the AF 555 channel disabled. Line-scans (8–10 pixels wide) were drawn perpendicular to the long axis on areas of the Golgi showing maximal separation of GM130 and TGN46. Line-scans were used if they resulted in a single clearly discernable peak in all three channels. The relative distance of the peak intensity of the protein of interest compared to the peak intensities of GM130 and TGN46 was then used to determine intra-Golgi localization.

Immunoblotting

Immunoblotting was performed as described (*Demetriou et al., 2001; Lee et al., 2007; Grigorian et al., 2007*). Antibodies against GM130 (610822), GS27 (611034), GS28 (611184), and STX6 (610635) were from BD Biosciences. The TGN46 antibodies used for immunoprecipitation (T7576) and immunoblotting (SAB4200235) were from Sigma, and the antibody against B3GNT2 was from Origene (TA505283).

Statistical analysis

Statistics were calculated with Prism software (GraphPad). *P* values were from two- or one-tailed unpaired *t*-tests (with Welch's correction). The Bonferroni correction was applied to all multiple comparisons. No statistical method was used to predetermine sample size. The experiments were not randomized.

Acknowledgements

Research was supported by the National Institute of Allergy and Infectious Diseases (R01AI053331, R01AI108917) and National Center for Complementary and Integrative Health (R01AT007452) to MD. HM was supported by National Heart, Lung, and Blood Institute of the National Institutes of Health under award number F30HL108451. Mass spectroscopy work was supported by the Biotechnology and Biological Sciences Research Council grant BB/K016164/1 (to AD and SMH). AD is a Wellcome Trust Senior Investigator. We thank Jesse Rodriguez for artistic assistance and Adeela Syed, John Greaves, Beniam Berhane and the UCI Genomics High-Throughput Facility for technical assistance.

Additional information

Funding

Funder	Grant reference number	Author
National Heart, Lung, and Blood Institute	F30HL108451	Haik Mkhikian
Biotechnology and Biological Sciences Research Council	BB/K016164/1	Stuart M Haslam Anne Dell

Wellcome Trust		Anne Dell
National Institute of Allergy and Infectious Diseases	R01AI053331	Michael Demetriou
National Center for Complementary and Integrative Health	R01AT007452	Michael Demetriou
National Institute of Allergy and Infectious Diseases	R01AI108917	Michael Demetriou

The funders had no role in study design, data collection and interpretation, or the decision to submit the work for publication.

Author contributions

HM, Conception and design, Acquisition of data, Analysis and interpretation of data, Drafting or revising the article; C-LM, RWZ, KK, GW, PK, Acquisition of data, Analysis and interpretation of data; SMH, AD, Acquisition of data, Analysis and interpretation of data, Drafting or revising the article; MD, Conception and design, Analysis and interpretation of data, Drafting or revising the article

Author ORCIDs

Michael Demetriou,  <http://orcid.org/0000-0001-8547-5774>

Ethics

Human subjects: Informed consent was obtained from human subjects to obtain peripheral blood for isolation of T cells and that resulting publications and/or presentations will not contain identifiable information. This was approved by the University of California Irvine Institutional Review board (HS#2001-2075).

Animal experimentation: This study was performed in strict accordance with the recommendations in the Guide for the Care and Use of Laboratory Animals of the National Institutes of Health. All of the animals were handled according to approved institutional animal care and use committee (IACUC) protocols (#2001-2305) of the University of California, Irvine.

References

- Ahmad N, Gabius HJ, André S, Kaltner H, Sabesan S, Roy R, Liu B, Macaluso F, Brewer CF. 2004. Galectin-3 precipitates as a pentamer with synthetic multivalent carbohydrates and forms heterogeneous cross-linked complexes. *Journal of Biological Chemistry* **279**:10841–10847. doi: [10.1074/jbc.M312834200](https://doi.org/10.1074/jbc.M312834200)
- Antonopoulos A, Demotte N, Stroobant V, Haslam SM, van der Bruggen P, Dell A. 2012. Loss of effector function of human cytolytic T lymphocytes is accompanied by major alterations in N- and O-glycosylation. *Journal of Biological Chemistry* **287**:11240–11251. doi: [10.1074/jbc.M111.320820](https://doi.org/10.1074/jbc.M111.320820)
- Barthel SR, Antonopoulos A, Cedeno-Laurent F, Schaffer L, Hernandez G, Patil SA, North SJ, Dell A, Matta KL, Neelamegham S, Haslam SM, Dimitroff CJ. 2011. Peracetylated 4-fluoro-glucosamine reduces the content and repertoire of N- and O-glycans without direct incorporation. *Journal of Biological Chemistry* **286**:21717–21731. doi: [10.1074/jbc.M110.194597](https://doi.org/10.1074/jbc.M110.194597)
- Beheshti Zavareh R, Sukhai MA, Hurren R, Gronda M, Wang X, Simpson CD, Maclean N, Zih F, Ketela T, Swallow CJ, Moffat J, Rose DR, Schachter H, Schimmer AD, Dennis JW. 2012. Suppression of cancer progression by MGAT1 shRNA knockdown. *PLoS One* **7**:e43721. doi: [10.1371/journal.pone.0043721](https://doi.org/10.1371/journal.pone.0043721)
- Beznoussenko GV, Parashuraman S, Rizzo R, Polishchuk R, Martella O, Di Giandomenico D, Fusella A, Spaar A, Sallese M, Capestrano MG, Pavelka M, Vos MR, Rikers YG, Helms V, Mironov AA, Luini A. 2014. Transport of soluble proteins through the Golgi occurs by diffusion via continuities across cisternae. *eLife* **3**:e02009. doi: [10.7554/eLife.02009](https://doi.org/10.7554/eLife.02009)
- Brewer CF, Miceli MC, Baum LG. 2002. Clusters, bundles, arrays and lattices: novel mechanisms for lectin-saccharide-mediated cellular interactions. *Current Opinion in Structural Biology* **12**:616–623. doi: [10.1016/S0959-440X\(02\)00364-0](https://doi.org/10.1016/S0959-440X(02)00364-0)
- Chen HL, Li CF, Grigorian A, Tian W, Demetriou M. 2009. T cell receptor signaling co-regulates multiple Golgi genes to enhance N-glycan branching. *Journal of Biological Chemistry* **284**:32454–32461. doi: [10.1074/jbc.M109.023630](https://doi.org/10.1074/jbc.M109.023630)
- Croci DO, Cerliani JP, Dalotto-Moreno T, Méndez-Huergo SP, Mascanfroni ID, Dergan-Dylon S, Toscano MA, Caramelo JJ, García-Vallejo JJ, Ouyang J, Mesri EA, Junttila MR, Bais C, Shipp MA, Salatino M, Rabinovich GA. 2014. Glycosylation-dependent lectin-receptor interactions preserve angiogenesis in anti-VEGF refractory tumors. *Cell* **156**:744–758. doi: [10.1016/j.cell.2014.01.043](https://doi.org/10.1016/j.cell.2014.01.043)

- Cummings RD**, Kornfeld S. 1982. Characterization of the structural determinants required for the high affinity interaction of asparagine-linked oligosaccharides with immobilized Phaseolus vulgaris leucoagglutinating and erythroagglutinating lectins. *Journal of Biological Chemistry* **257**:11230–11234.
- Dam TK**, Brewer CF. 2010. Lectins as pattern recognition molecules: the effects of epitope density in innate immunity. *Glycobiology* **20**:270–279. doi: [10.1093/glycob/cwp186](https://doi.org/10.1093/glycob/cwp186)
- Dejgaard SY**, Murshid A, Dee KM, Presley JF. 2007. Confocal microscopy-based linescan methodologies for intra-Golgi localization of proteins. *Journal of Histochemistry and Cytochemistry* **55**:709–719. doi: [10.1369/jhc.6A7090.2007](https://doi.org/10.1369/jhc.6A7090.2007)
- Demetriou M**, Granovsky M, Quaggin S, Dennis JW. 2001. Negative regulation of T-cell activation and autoimmunity by Mgat5 N-glycosylation. *Nature* **409**:733–739. doi: [10.1038/35055582](https://doi.org/10.1038/35055582)
- Dennis JW**, Brewer CF. 2013. Density-dependent lectin-glycan interactions as a paradigm for conditional regulation by posttranslational modifications. *Molecular & Cellular Proteomics* **12**:913–920. doi: [10.1074/mcp.R112.026989](https://doi.org/10.1074/mcp.R112.026989)
- Dennis JW**, Laferté S, Waghorne C, Breitman ML, Kerbel RS. 1987. Beta 1-6 branching of Asn-linked oligosaccharides is directly associated with metastasis. *Science* **236**:582–585. doi: [10.1126/science.2953071](https://doi.org/10.1126/science.2953071)
- Dennis JW**, Nabi IR, Demetriou M. 2009. Metabolism, cell surface organization, and disease. *Cell* **139**:1229–1241. doi: [10.1016/j.cell.2009.12.008](https://doi.org/10.1016/j.cell.2009.12.008)
- Fernandes B**, Sagman U, Auger M, Demetrio M, Dennis JW. 1991. Beta 1-6 branched oligosaccharides as a marker of tumor progression in human breast and colon neoplasia. *Cancer Research* **51**:718–723.
- Fukuda M**, Carlsson SR, Klock JC, Dell A. 1986. Structures of O-linked oligosaccharides isolated from normal granulocytes, chronic myelogenous leukemia cells, and acute myelogenous leukemia cells. *Journal of Biological Chemistry* **261**:12796–12806.
- Glick BS**, Luini A. 2011. Models for Golgi traffic: a critical assessment. *Cold Spring Harbor Perspectives in Biology* **3**:a005215. doi: [10.1101/cshperspect.a005215](https://doi.org/10.1101/cshperspect.a005215)
- Goss PE**, Baptiste J, Fernandes B, Baker M, Dennis JW. 1994. A phase I study of swainsonine in patients with advanced malignancies. *Cancer Research* **54**:1450–1457. doi: [10.1097/00002371-199311000-00053](https://doi.org/10.1097/00002371-199311000-00053)
- Goss PE**, Reid CL, Bailey D, Dennis JW. 1997. Phase IB clinical trial of the oligosaccharide processing inhibitor swainsonine in patients with advanced malignancies. *Clinical Cancer Research* **3**:1077–1086.
- Granovsky M**, Fata J, Pawling J, Muller WJ, Khokha R, Dennis JW. 2000. Suppression of tumor growth and metastasis in Mgat5-deficient mice. *Nature Medicine* **6**:306–312. doi: [10.1038/73163](https://doi.org/10.1038/73163)
- Grigorian A**, Araujo L, Naidu NN, Place DJ, Choudhury B, Demetriou M. 2011. N-acetylglucosamine inhibits T-helper 1 (Th1)/T-helper 17 (Th17) cell responses and treats experimental autoimmune encephalomyelitis. *Journal of Biological Chemistry* **286**:40133–40141. doi: [10.1074/jbc.M111.277814](https://doi.org/10.1074/jbc.M111.277814)
- Grigorian A**, Lee SU, Tian W, Chen IJ, Gao G, Mendelsohn R, Dennis JW, Demetriou M. 2007. Control of T Cell-mediated autoimmunity by metabolite flux to N-glycan biosynthesis. *Journal of Biological Chemistry* **282**:20027–20035. doi: [10.1074/jbc.M701890200](https://doi.org/10.1074/jbc.M701890200)
- Grigorian A**, Torossian S, Demetriou M. 2009. T-cell growth, cell surface organization, and the galectin-glycoprotein lattice. *Immunological Reviews* **230**:232–246. doi: [10.1111/j.1600-065X.2009.00796.x](https://doi.org/10.1111/j.1600-065X.2009.00796.x)
- Hirabayashi J**, Hashidate T, Arata Y, Nishi N, Nakamura T, Hirashima M, Urashima T, Oka T, Futai M, Muller WE, Yagi F, Kasai K. 2002. Oligosaccharide specificity of galectins: a search by frontal affinity chromatography. *Biochimica Et Biophysica Acta* **1572**:232–254. doi: [10.1016/S0304-4165\(02\)00311-2](https://doi.org/10.1016/S0304-4165(02)00311-2)
- Ioffe E**, Stanley P. 1994. Mice lacking N-acetylglucosaminyltransferase I activity die at mid-gestation, revealing an essential role for complex or hybrid N-linked carbohydrates. *Proceedings of the National Academy of Sciences of the United States of America* **91**:728–732. doi: [10.1073/pnas.91.2.728](https://doi.org/10.1073/pnas.91.2.728)
- Ishida H**, Togayachi A, Sakai T, Iwai T, Hiruma T, Sato T, Okubo R, Inaba N, Kudo T, Gotoh M, Shoda J, Tanaka N, Narimatsu H. 2005. A novel beta1,3-N-acetylglucosaminyltransferase (beta3Gn-T8), which synthesizes poly-N-acetyllactosamine, is dramatically upregulated in colon cancer. *FEBS Letters* **579**:71–78. doi: [10.1016/j.febslet.2004.11.037](https://doi.org/10.1016/j.febslet.2004.11.037)
- Ismail MN**, Stone EL, Panico M, Lee SH, Luu Y, Ramirez K, Ho SB, Fukuda M, Marth JD, Haslam SM, Dell A. 2011. High-sensitivity O-glycomic analysis of mice deficient in core 2 {beta}1,6-N-acetylglucosaminyltransferases. *Glycobiology* **21**:82–98. doi: [10.1093/glycob/cwq134](https://doi.org/10.1093/glycob/cwq134)
- Johswich A**, Longuet C, Pawling J, Abdel Rahman A, Ryczko M, Drucker DJ, Dennis JW. 2014. N-glycan remodeling on glucagon receptor is an effector of nutrient sensing by the hexosamine biosynthesis pathway. *Journal of Biological Chemistry* **289**:15927–15941. doi: [10.1074/jbc.M114.563734](https://doi.org/10.1074/jbc.M114.563734)
- Kawashima H**, Sueyoshi S, Li H, Yamamoto K, Osawa T. 1990. Carbohydrate binding specificities of several poly-N-acetyllactosamine-binding lectins. *Glycoconjugate Journal* **7**:323–334. doi: [10.1007/BF01073376](https://doi.org/10.1007/BF01073376)
- Kim S**, Miura Y, Etchison JR, Freeze HH. 2001. Intact Golgi synthesize complex branched O-linked chains on glycoside primers: evidence for the functional continuity of seven glycosyltransferases and three sugar nucleotide transporters. *Glycoconjugate Journal* **18**:623–633. doi: [10.1023/A:1020691619908](https://doi.org/10.1023/A:1020691619908)
- Kornfeld R**, Kornfeld S. 1985. Assembly of asparagine-linked oligosaccharides. *Annual Review of Biochemistry* **54**:631–664. doi: [10.1146/annurev.bi.54.070185.003215](https://doi.org/10.1146/annurev.bi.54.070185.003215)
- Lau KS**, Partridge EA, Grigorian A, Silvescu CI, Reinhold VN, Demetriou M, Dennis JW. 2007. Complex N-glycan number and degree of branching cooperate to regulate cell proliferation and differentiation. *Cell* **129**:123–134. doi: [10.1016/j.cell.2007.01.049](https://doi.org/10.1016/j.cell.2007.01.049)
- Lee SU**, Grigorian A, Pawling J, Chen IJ, Gao G, Mozaffar T, McKerlie C, Demetriou M. 2007. N-glycan processing deficiency promotes spontaneous inflammatory demyelination and neurodegeneration. *Journal of Biological Chemistry* **282**:33725–33734. doi: [10.1074/jbc.M704839200](https://doi.org/10.1074/jbc.M704839200)

- Li CF, Zhou RW, Mkhikian H, Newton BL, Yu Z, Demetriou M. 2013. Hypomorphic MGAT5 polymorphisms promote multiple sclerosis cooperatively with MGAT1 and interleukin-2 and 7 receptor variants. *Journal of Neuroimmunology* **256**:71–76. doi: [10.1016/j.jneuroim.2012.12.008](https://doi.org/10.1016/j.jneuroim.2012.12.008)
- Maley F, Trimble RB, Tarentino AL, Plummer TH. 1989. Characterization of glycoproteins and their associated oligosaccharides through the use of endoglycosidases. *Analytical Biochemistry* **180**:195–204. doi: [10.1016/0003-2697\(89\)90115-2](https://doi.org/10.1016/0003-2697(89)90115-2)
- Martínez-Alonso E, Tomás M, Martínez-Menárguez JA. 2013. Golgi tubules: their structure, formation and role in intra-Golgi transport. *Histochemistry and Cell Biology* **140**:327–339. doi: [10.1007/s00418-013-1114-9](https://doi.org/10.1007/s00418-013-1114-9)
- Merkle RK, Cummings RD. 1987. Relationship of the terminal sequences to the length of poly-N-acetyllactosamine chains in asparagine-linked oligosaccharides from the mouse lymphoma cell line BW5147. Immobilized tomato lectin interacts with high affinity with glycopeptides containing long poly-N-acetyllactosamine chains. *Journal of Biological Chemistry* **262**:8179–8189.
- Metzler M, Gertz A, Sarkar M, Schachter H, Schrader JW, Marth JD. 1994. Complex asparagine-linked oligosaccharides are required for morphogenic events during post-implantation development. *The EMBO Journal* **13**:2056–2065.
- Mkhikian H, Grigorian A, Li CF, Chen HL, Newton B, Zhou RW, Beeton C, Torossian S, Tatarian GG, Lee SU, Lau K, Walker E, Siminovitch KA, Chandy KG, Yu Z, Dennis JW, Demetriou M. 2011. Genetics and the environment converge to dysregulate N-glycosylation in multiple sclerosis. *Nature Communications* **2**:334. doi: [10.1038/ncomms1333](https://doi.org/10.1038/ncomms1333)
- National Academy of Sciences. 2012. *Transforming Glycoscience: A Roadmap for the Future*. Washington, DC: National Academies Press
- Oguri S. 2005. Analysis of sugar chain-binding specificity of tomato lectin using lectin blot: recognition of high mannose-type N-glycans produced by plants and yeast. *Glycoconjugate Journal* **22**:453–461. doi: [10.1007/s10719-005-5329-4](https://doi.org/10.1007/s10719-005-5329-4)
- Ohtsubo K, Takamatsu S, Minowa MT, Yoshida A, Takeuchi M, Marth JD. 2005. Dietary and genetic control of glucose transporter 2 glycosylation promotes insulin secretion in suppressing diabetes. *Cell* **123**:1307–1321. doi: [10.1016/j.cell.2005.09.041](https://doi.org/10.1016/j.cell.2005.09.041)
- Partridge EA, Le Roy C, Di Guglielmo GM, Pawling J, Cheung P, Granovsky M, Nabi IR, Wrana JL, Dennis JW. 2004. Regulation of cytokine receptors by Golgi N-glycan processing and endocytosis. *Science* **306**:120–124. doi: [10.1126/science.1102109](https://doi.org/10.1126/science.1102109)
- San Pietro E, Capestrano M, Polishchuk EV, DiPentima A, Trucco A, Zizza P, Mariggio S, Pulvirenti T, Sallèse M, Tete S, Mironov AA, Leslie CC, Corda D, Luini A, Polishchuk RS. 2009. Group IV phospholipase A(2)alpha controls the formation of inter-cisternal continuities involved in intra-Golgi transport. *PLoS Biology* **7**:e1000194. doi: [10.1371/journal.pbio.1000194](https://doi.org/10.1371/journal.pbio.1000194)
- Schachter H. 1986. Biosynthetic controls that determine the branching and microheterogeneity of protein-bound oligosaccharides. *Biochemistry and Cell Biology* **64**:163–181. doi: [10.1139/o86-026](https://doi.org/10.1139/o86-026)
- Schachter H. 1991. The 'yellow brick road' to branched complex N-glycans. *Glycobiology* **1**:453–461. doi: [10.1093/glycob/1.5.453](https://doi.org/10.1093/glycob/1.5.453)
- Stone EL, Ismail MN, Lee SH, Luu Y, Ramirez K, Haslam SM, Ho SB, Dell A, Fukuda M, Marth JD. 2009. Glycosyltransferase function in core 2-type protein O glycosylation. *Molecular and Cellular Biology* **29**:3770–3782. doi: [10.1128/MCB.00204-09](https://doi.org/10.1128/MCB.00204-09)
- Takamatsu S, Antonopoulos A, Ohtsubo K, Ditto D, Chiba Y, Le DT, Morris HR, Haslam SM, Dell A, Marth JD, Taniguchi N. 2010. Physiological and glycomic characterization of N-acetylglucosaminyltransferase-IVa and -IVb double deficient mice. *Glycobiology* **20**:485–497. doi: [10.1093/glycob/cwp200](https://doi.org/10.1093/glycob/cwp200)
- Togayachi A, Kozono Y, Ishida H, Abe S, Suzuki N, Tsunoda Y, Hagiwara K, Kuno A, Ohkura T, Sato N, Sato T, Hirabayashi J, Ikehara Y, Tachibana K, Narimatsu H. 2007. Polylactosamine on glycoproteins influences basal levels of lymphocyte and macrophage activation. *Proceedings of the National Academy of Sciences of the United States of America* **104**:15829–15834. doi: [10.1073/pnas.0707426104](https://doi.org/10.1073/pnas.0707426104)
- Trucco A, Polishchuk RS, Martella O, Di Pentima A, Fusella A, Di Giandomenico D, San Pietro E, Beznoussenko GV, Polishchuk EV, Baldassarre M, Buccione R, Geerts WJ, Koster AJ, Burger KN, Mironov AA, Luini A. 2004. Secretory traffic triggers the formation of tubular continuities across Golgi sub-compartments. *Nature Cell Biology* **6**:1071–1081. doi: [10.1038/ncb1180](https://doi.org/10.1038/ncb1180)
- Wang D, Xu L, Lv L, Su LY, Fan Y, Zhang DF, Bi R, Yu D, Zhang W, Li XA, Li YY, Yao YG. 2015. Association of the LRRK2 genetic polymorphisms with leprosy in Han Chinese from Southwest China. *Genes and Immunity* **16**:112–119. doi: [10.1038/gene.2014.72](https://doi.org/10.1038/gene.2014.72)
- Wang Y, Tan J, Sutton-Smith M, Ditto D, Panico M, Campbell RM, Varki NM, Long JM, Jaeken J, Levinson SR, Wynshaw-Boris A, Morris HR, Le D, Dell A, Schachter H, Marth JD. 2001. Modeling human congenital disorder of glycosylation type IIa in the mouse: conservation of asparagine-linked glycan-dependent functions in mammalian physiology and insights into disease pathogenesis. *Glycobiology* **11**:1051–1070. doi: [10.1093/glycob/11.12.1051](https://doi.org/10.1093/glycob/11.12.1051)
- Watanabe K, Hakomori SI, Childs RA, Feizi T. 1979. Characterization of a blood group I-active ganglioside. Structural requirements for I and i specificities. *Journal of Biological Chemistry* **254**:3221–3228.
- Ye Z, Marth JD. 2004. N-glycan branching requirement in neuronal and postnatal viability. *Glycobiology* **14**:547–558. doi: [10.1093/glycob/cwh069](https://doi.org/10.1093/glycob/cwh069)
- Zhao W, Chen TL, Vertel BM, Colley KJ. 2006. The CMP-sialic acid transporter is localized in the medial-trans Golgi and possesses two specific endoplasmic reticulum export motifs in its carboxyl-terminal cytoplasmic tail. *Journal of Biological Chemistry* **281**:31106–31118. doi: [10.1074/jbc.M605564200](https://doi.org/10.1074/jbc.M605564200)

Zhou RW, Mkhikian H, Grigorian A, Hong A, Chen D, Arakelyan A, Demetriou M. 2014. N-glycosylation bidirectionally extends the boundaries of thymocyte positive selection by decoupling Lck from Ca^{2+} signaling. *Nature Immunology* **15**:1038–1045. doi: [10.1038/ni.3007](https://doi.org/10.1038/ni.3007)